

**ISTANBUL TECHNICAL UNIVERSITY ★ GRADUATE SCHOOL OF SCIENCE**  
**ENGINEERING AND TECHNOLOGY**

**INVESTIGATION OF TWO DIMENSIONAL MATERIALS WITH  
SIMULTANEOUS ATOMIC FORCE/SCANNING TUNNELING  
MICROSCOPY**



**Ph.D. THESIS**

**Majid FAZELI JADIDI**

**Department of Physics Engineering**

**Physics Engineering Programme**

**JANUARY 2019**



**ISTANBUL TECHNICAL UNIVERSITY ★ GRADUATE SCHOOL OF SCIENCE**  
**ENGINEERING AND TECHNOLOGY**

**INVESTIGATION OF TWO DIMENSIONAL MATERIALS WITH  
SIMULTANEOUS ATOMIC FORCE/SCANNING TUNNELING  
MICROSCOPY**



**Ph.D. THESIS**

**Majid FAZELI JADIDI**  
**(509122117)**

**Department of Physics Engineering**

**Physics Engineering Programme**

**Thesis Advisor: Assoc. Prof. Hakan Özgür ÖZER**

**JANUARY 2019**



**İSTANBUL TEKNİK ÜNİVERSİTESİ ★ FEN BİLİMLERİ ENSTİTÜSÜ**

**İKİ BOYUTLU MALZEMELERİN EŞZAMANLI  
ATOMİK KUVVET / TARAMALI TÜNELLEME MİKROSKOBU  
İLE İNCELENMESİ**

**DOKTORA TEZİ**

**Majid FAZELI JADIDI  
(509122117)**

**Fizik Mühendisliği Anabilim Dalı**

**Fizik Mühendisliği Programı**

**Tez Danışmanı: Doç. Dr. Hakan Özgür ÖZER**

**OCAK 2019**



Majid Fazeli Jadidi, a Ph.D. student of İTÜ Graduate School of Science Engineering and Technology student ID 509122117, successfully defended the thesis/dissertation entitled “INVESTIGATION OF TWO DIMENSIONAL MATERIALS WITH SIMULTANEOUS ATOMIC FORCE/SCANNING TUNNELING MICROSCOPY”, which he prepared after fulfilling the requirements specified in the associated legislations, before the jury whose signatures are below.

**Thesis Advisor :**      **Assoc. Prof. Hakan Özgür ÖZER** .....  
İstanbul Technical University

**Jury Members :**      **Prof. Dr. Ahmet ORAL** .....  
Middle East Technical University

**Assoc. Prof. Oğuzhan GÜRLÜ** .....  
İstanbul Technical University

**Prof. Dr. Ferid SALEHLİ** .....  
İstanbul Technical University

**Assoc. Prof. Kaan Güven** .....  
Koç University

**Date of Submission : 07 . 12 . 2018**

**Date of Defense : 04 . 01 . 2019**







*To my mother and father,*



## **FOREWORD**

I would like to express my profound thanks to my supervisor Assoc. Prof. H. Özgür ÖZER for his guidance, friendship and great support. He was always my source of inspiration by his hard work, dedication, patience and valuable advice.

I would also like to thank NanoMagnetics Instruments for providing technical supply. I would like to express my endless thanks to Ipen Demirel and Ahmed Uluca for their help, motivation and support.

Finally, I am grateful to my beloved family for their support in every period of my life.

January 2019

Majid FAZELI JADIDI



## TABLE OF CONTENTS

	<u>Page</u>
<b>FOREWORD</b> .....	<b>ix</b>
<b>TABLE OF CONTENTS</b> .....	<b>xi</b>
<b>ABBREVIATIONS</b> .....	<b>xiii</b>
<b>SYMBOLS</b> .....	<b>xv</b>
<b>LIST OF FIGURES</b> .....	<b>xvii</b>
<b>SUMMARY</b> .....	<b>xxi</b>
<b>ÖZET</b> .....	<b>xxiii</b>
<b>1. INTRODUCTION</b> .....	<b>1</b>
1.1 Purpose of Thesis .....	3
1.2 Literature Review .....	4
1.2.1 Highly oriented pyrolytic graphite (HOPG).....	4
1.2.2 Graphene .....	5
<b>2. METHODS AND EQUIPMENTS</b> .....	<b>11</b>
2.1 Scanning Tunneling Microscopy .....	11
2.2 Atomic Force Microscopy .....	12
2.3 Simultaneous STM/AFM .....	15
2.3.1 Fiber optic interferometer setup .....	16
2.3.2 Calibration of cantilever .....	18
2.3.3 Channels of microscope .....	19
2.3.4 Force-distance spectroscopy.....	21
2.4 Ultra High Vacuum Unit .....	21
<b>3. SYNTHESIS OF GRAPHENE</b> .....	<b>23</b>
3.1 CVD Grown Graphene .....	23
3.2 Transferring of CVD Grown Graphene on SiO <sub>2</sub> .....	24
<b>4. RESULTS AND DISCUSSION</b> .....	<b>27</b>
4.1 Graphene on Cu.....	27
4.1.1 Results obtained by Si cantilever .....	27
4.1.2 Results obtained by W cantilever .....	37
4.1.3 Comparison of results obtained by W and Si cantilevers.....	45
4.2 Graphene Transferred on SiO <sub>2</sub> .....	45
4.3 Bismuth Telluride (Bi <sub>2</sub> Te <sub>3</sub> ) .....	46
<b>5. CONCLUSIONS</b> .....	<b>49</b>
<b>REFERENCES</b> .....	<b>53</b>
<b>CURRICULUM VITAE</b> .....	<b>57</b>



## **ABBREVIATIONS**

<b>STM</b>	: Scanning Tunneling Microscope
<b>AFM</b>	: Atomic Force Microscope
<b>SPM</b>	: Scanning Probe Microscopy
<b>UHV</b>	: Ultra High Vacuum
<b>CVD</b>	: Chemical Vapor Deposition
<b>HOPG</b>	: Highly Oriented Pyrolytic Graphite
<b>PMMA</b>	: PolyMethyl MethAcrylate







## SYMBOLS

$\text{\AA}$	: Ångström
<b>nA</b>	: nanoAmper
<b>z</b>	: Tip-surface distance
<b>V</b>	: Volt
<b>p-p</b>	: peak to peak
<b>rms</b>	: root mean square
<b>V<sub>sample</sub></b>	: Bias voltage on sample
<b>I<sub>t</sub></b>	: Tunnel current
<b>A<sub>0</sub></b>	: Free oscillation amplitude
<b><math>\omega_0</math></b>	: Resonance frequency
<b><math>\omega</math></b>	: Excitation frequency
<b><math>\phi</math></b>	: Barrier height
<b>k</b>	: Stiffness
<b>W</b>	: Tungsten
<b>Hz</b>	: Hertz
<b><math>\kappa</math></b>	: Decay constant
<b>K</b>	: Kelvin



## LIST OF FIGURES

	<u>Page</u>
<b>Figure 1.1</b> : Schematics of bilayer graphene and a unit cell.....	2
<b>Figure 1.2</b> : Schematic of two layers of HOPG. (a) Normal stacking where A atoms and B atoms are indicated by open circles and solid circles respectively. (b) Top layer was shifted without rotation. (c) Top layer was shifted with a rotation. In this situation, the Moiré' pattern can be seen in STM topography, taken from ref. [10].....	4
<b>Figure 1.3</b> : Typical STM image of Moiré' pattern on HOPG surface (50 nm × 50 nm) and an enlarged zone (6 nm x 6 nm), taken from ref. [10].....	5
<b>Figure 1.4</b> : Force as function of tip-surface distance are calculated on carbon atoms (open symbols) and hollow sites (solid symbols) for a) Ir b) Pt c) H3 Si d) dimer terminated Si and e) W tips, taken from ref. [25]... ..	7
<b>Figure 1.5</b> : STM image of graphene on Ir (111). The moiré patterns result from the superposition of the graphene lattice with the lattice of the underlying metal surface. The image size is 15 nm × 15 nm, taken from ref. [22]....	8
<b>Figure 1.6</b> : Drawing schematics of the edge structures in graphene sheet and nanoribbon. (Image courtesy of M. Hofmann, MIT).....	8
<b>Figure 1.7</b> : Triangular and hexagonal shapes of zigzag edges are formed by atoms that belong to the same sublattice, A or B type, taken from ref. [40].....	9
<b>Figure 2.1</b> : Drawing schematic of the quantum tunneling in STM setup.....	11
<b>Figure 2.2</b> : Drawing schematic of typical STM setup.. ..	12
<b>Figure 2.3</b> : Drawing schematic of typical AFM setup.....	13
<b>Figure 2.4</b> : Typical Force-Distance curve between two atoms and indicated operating regimes in different AFM modes ... ..	14
<b>Figure 2.5</b> : Resonance frequency shift of cantilever during the interaction with sample in the attractive and repulsive force regimes.....	15
<b>Figure 2.6</b> : Head of home-built simultaneous AFM/STM.....	16
<b>Figure 2.7</b> : Schematics of AFM/STM microscope and Fabry-Prot fiber interferometer taken from ref. [42].....	17
<b>Figure 2.8</b> : Typical interference pattern obtained with W cantilever. The most sensitive point is indicated by arrow with the maximum slope of (-107.98 mV/Å).....	18
<b>Figure 2.9</b> : Fit of the thermal resonance curve of the W cantilever on the Brownian noise curve, calculated stiffness of $k \approx 53$ N/m.....	19
<b>Figure 2.10</b> : AFM/STM in Ultra High Vacuum.. ..	22
<b>Figure 3.1</b> : Schematic of CVD process for growth of graphene on Cu foil. ....	23
<b>Figure 3.2</b> : Schematic shows PMMA technique, which is used to transfer graphene on the target substrate. ....	24
<b>Figure 3.3</b> : Raman spectroscopy results of singlelayer and multilayer graphene transferred on SiO2 wafer surface. ....	25
<b>Figure 4.1</b> : STM topography images of (a) region with different steps, (b) and (c) upper region of image (a) which seems to be single layer graphene, (d) a region that both honeycomb and hexagonal pattern are observed that could	

- be a border of single layer and multilayer graphene. Obtained with a Pt-Ir coated Si tip. Image sizes are  $380 \times 380 \text{ \AA}^2$ ,  $43 \times 43 \text{ \AA}^2$ ,  $43 \times 43 \text{ \AA}^2$  and  $29 \times 29 \text{ \AA}^2$  respectively. .... Error! Bookmark not defined. **28**
- Figure 4.2 :** (a) Trigonal pattern in STM topography (b) Honeycomb pattern in inverted contrast of STM topography. Obtained using a Pt-Ir coated Si tip. Image size is  $58 \times 58 \text{ \AA}^2$ .  $V_{\text{sample}} = -0.05 \text{ V}$ ,  $I_t = 0.2 \text{ nA}$  ... ..... **29**
- Figure 4.3 :** Effect of tip changes during a particular scan is shown in (a) Tunnel current modulation and (b) STM topography images. Obtained using a Pt-Ir coated Si tip. Image size is  $29 \times 29 \text{ \AA}^2$ .  $V_{\text{sample}} = -0.15 \text{ V}$ ,  $I_t = 0.2 \text{ nA}$ , free amplitude  $A_0 = 0.41 \text{ \AA}_{\text{rms}}$ . .... **29**
- Figure 4.4 :** Simultaneous AFM/STM images of graphene surface. (a) Oscillation amplitude (inverted contrast of force gradient) in constant tunnel current mode (b) Zoomed region of oscillation amplitude image (c) STM topography in constant current mode (d) Inverted contrast of STM topography (e) Zoomed region of inverted STM topography image. Obtained by Si cantilever.  $f = 51.4 \text{ kHz}$ . Image size is  $58 \times 58 \text{ \AA}^2$ .  $V_{\text{sample}} = -50 \text{ mV}$ ,  $I_t = 0.2 \text{ nA}$ , free oscillation amplitude  $A_0 = 0.354 \text{ \AA}_{\text{rms}}$ . ..... **30**
- Figure 4.5 :** Simultaneous AFM / STM images of Graphene surface and the corresponded zoomed regions. (a) Tunnel current modulation amplitude (measure of the tunnel barrier height), the inverted contrast was displayed as well. (b) Oscillation amplitude (inverted contrast of force gradient) (c) Phase shift (measure of energy loss) (d) STM topography, Obtained using Pt-Ir coated Si cantilever.  $k = 40 \text{ N/m}$ ,  $f = 47 \text{ kHz}$ , Image size is  $44 \times 44 \text{ \AA}^2$ .  $V_{\text{sample}} = 0.2 \text{ V}$ ,  $I_t = 0.17 \text{ nA}$ , free oscillation amplitude  $A_0 = 0.56 \text{ \AA}_{\text{rms}}$ . .... **32**
- Figure 4.6 :** Honeycomb models overlaid on the selected regions shown in Figure 4.5 (a) Inverted contrast of tunnel current modulation amplitude (b) Oscillation amplitude (inverted contrast of force gradient) (c) Phase shift (measure of energy dissipation) (d) Inverted contrast of STM topography.)..... **33**
- Figure 4.7 :** Simultaneous AFM / STM images of the graphene surface. (A) STM topography (b) tunnel current modulation amplitude (measure of the tunnel barrier height) (c) oscillation amplitude (inverted contrast of force gradient). The following series are enlarged areas of frame shown in (a). Elements such as lateral shift and pixel delay has been corrected in the images. Obtained using Si cantilever.  $f = 51.4 \text{ kHz}$ . Image size is  $29 \times 29 \text{ \AA}^2$ .  $V_{\text{sample}} = -70 \text{ mV}$ ,  $I_t = 0.2 \text{ nA}$ , Free amplitude  $A_0 = 0.31 \text{ \AA}_{\text{rms}}$ . ..... **34**
- Figure 4.8 :** F-d Spectroscopy. The Force, Phase shift and tunnel current curves as a result of sample displacement. Obtained by Si cantilever with the stiffness of  $(40 \text{ N/m})$  on the graphene surface..  $f = 47 \text{ kHz}$ .  $f_0 = 156940 \text{ Hz}$ .  $A_0 = 0.48 \text{ \AA}_{\text{rms}}$ ,  $V_{\text{sample}} = -0.3 \text{ V}$ . .... **35**
- Figure 4.9 :** Simultaneous AFM/STM images of graphene surface. (a) Oscillation amplitude in constant current mode (b) Oscillation amplitude in constant height mode (c) STM topography in constant tunnel current mode (d) STM topography in constant height mode. Obtained using Si cantilever.  $f = 51.4 \text{ kHz}$ . Image size is  $58 \times 58 \text{ \AA}^2$ .  $V_{\text{sample}} = 50 \text{ mV}$ ,  $I_t = 0.2 \text{ nA}$ , free oscillation amplitude  $A_0 = 0.32 \text{ \AA}_{\text{rms}}$ . .... **36**
- Figure 4.10 :** STM image of Graphene surface on Cu substrate. Obtained using a W tip Image size is  $820 \times 820 \text{ nm}^2$ .  $V_{\text{sample}} = -0.7 \text{ V}$ ,  $I_t = 0.2 \text{ nA}$ . .... **37**

- Figure 4.11** : Simultaneous AFM/STM images of border of bilayer Graphene. (a) STM topography in constant current (forward scan) (b) Interaction Stiffness in constant height mode (backward scan). A pair of hexagonal unit cells is superimposed on the images. W cantilever of stiffness  $k = 53$  N/m and resonance frequency  $f_0=31.5$  kHz. Drive frequency  $f = 15$  kHz. Image size is  $18 \times 10 \text{ \AA}^2$ ,  $V_{\text{sample}} = 0.5$  V,  $I_t = 0.6$  nA, Free amplitude  $A_0 = 0.3 \text{ \AA}_{\text{rms}}$ . ..... **38**
- Figure 4.12** : Simultaneous AFM/STM images of Graphene surface on Cu substrate. (a) STM topography in constant current (forward scan) (b) Barrier height (eV) in constant height mode (backward scan). (c) Energy dissipation (eV) per oscillation cycle in constant height mode. (d) Interaction Stiffness in constant current mode (forward scan) and (e) Interaction Stiffness in constant height mode (backward scan). Scale bar values are in units of  $\text{\AA}$  in STM and N/m in interaction stiffness images. Obtained with a W tip and cantilever of stiffness  $k = 53$  N/m and resonance frequency  $f_0=31.5$  kHz. Drive frequency  $f = 15$  kHz. Image size is  $11 \times 11 \text{ \AA}^2$ ,  $V_{\text{sample}} = -0.5$  V,  $I_t = 1.2$  nA, Free amplitude  $A_0 = 0.3 \text{ \AA}_{\text{rms}}$ . ..... **40**
- Figure 4.13** : Simultaneous AFM/STM images of Graphene surface on Cu substrate. (a) STM topography in constant current (forward scan) (b) Interaction Stiffness in constant current mode (forward scan) and (c) Interaction Stiffness in constant height mode (backward scan). Scale bar values are in units of  $\text{\AA}$  in STM and N/m in interaction stiffness images. Obtained with a W tip and cantilever of stiffness  $k = 53$  N/m and resonance frequency  $f_0=31.5$  kHz. Drive frequency  $f = 15$  kHz. Image size is  $11 \times 11 \text{ \AA}^2$ ,  $V_{\text{sample}} = 0.5$  V,  $I_t = 1.2$  nA, Free amplitude  $A_0 = 0.3 \text{ \AA}_{\text{rms}}$ . ..... **41**
- Figure 4.14** : Simultaneous AFM/STM images of Graphene surface. (a) STM topography in constant current (forward scan) (b) Interaction Stiffness in constant height mode (backward scan). A pair of hexagonal unit cells is superimposed on the images. The profiles along the indicated lines are given in (c) and (d). W cantilever of stiffness  $k = 53$  N/m and resonance frequency  $f_0=31.5$  kHz. Drive frequency  $f = 15$  kHz. Image size is  $18 \times 18 \text{ \AA}^2$ ,  $V_{\text{sample}} = 0.5$  V,  $I_t = 0.6$  nA, Free amplitude  $A_0 = 0.3 \text{ \AA}_{\text{rms}}$  ... ..... **42**
- Figure 4.15** : F-d Spectroscopy. The Force (F) and Tunnel current ( I ) were measured as a function of relative tip-sample displacement, on a carbon site (blue curves) and hollow site (red curves). Obtained using the W cantilever used in imaging experiments, with stiffness of 53 N/m.  $V_{\text{sample}} = 0.5$  V ... ..... **43**
- Figure 4.16** : F-d Spectroscopy. The Force (F) and Tunnel current ( I ) were measured as a function of relative tip-sample displacement, on a carbon site (blue curves) and hollow site (red curves). Obtained using the W cantilever used in imaging experiments, with stiffness of 53 N/m.  $V_{\text{sample}} = -0.35$  V. **44**
- Figure 4.17** : AFM/STM images of Graphene surface. (a) STM topography in constant current mode with bias voltage of  $-0.35$  V (b) STM topography in constant current mode with bias voltage of  $-0.4$  V (c) Inverted contrast of oscillation amplitude (force gradient) constant current mode with bias voltage of  $-0.4$  V. Obtained using W cantilever of stiffness  $k = 53$  N/m and resonance frequency  $f_0=31.5$  kHz. Drive frequency  $f = 15$  kHz. Image size is  $29 \times 29 \text{ \AA}^2$ ,  $I_t = 0.4$  nA, Free amplitude  $A_0 = 0.3 \text{ \AA}_{\text{rms}}$  ..... **44**
- Figure 4.18** : Simultaneous AFM/STM images of graphene surface on SiO<sub>2</sub> (a Tunnel current modulation amplitude (measure of the tunnel barrier height) (b)

Oscillation amplitude (measure of force gradient) (c) STM topography obtained using Si cantilever.  $f = 18.340$  kHz. Image size is  $25 \times 25 \text{ \AA}^2$ .  $V_{\text{sample}} = -850$  mV,  $I_t = 0.15$  nA, free oscillation amplitude  $A_0 = 0.22 \text{ \AA}$  rms ... 46

**Figure 4.19** : Simultaneous AFM/STM images of Bi<sub>2</sub>Te<sub>3</sub>. (a) Tunnel current modulation amplitude (measure of the tunnel barrier height) (b) Oscillation amplitude (measure of force gradient) (c) STM topography obtained using Si cantilever.  $f = 24.807$  kHz. Image size is  $35 \times 35 \text{ \AA}^2$ .  $V_{\text{sample}} = -1$  V,  $I_t = 0.25$  nA, free oscillation amplitude  $A_0 = 0.69 \text{ \AA}$  rms ... 47



# INVESTIGATION OF TWO DIMENSIONAL MATERIALS WITH SIMULTANEOUS ATOMIC FORCE/SCANNING TUNNELING MICROSCOPY

## SUMMARY

In this study, two-dimensional materials particularly CVD-grown graphene on copper foil, were investigated using simultaneous Atomic Force/Scanning Tunneling Microscopy (AFM/STM). This is probably the first demonstration of truly simultaneous AFM/STM imaging of graphene with emphasis to atomic scale contrast, since we use very small oscillation amplitudes in assessing force gradient interaction. The use of large amplitudes results in tip being in tunneling regime only in a small fraction of its oscillation cycle and this does not resemble true STM operation. The STM investigation of HOPG, usually revealing triangular atomic patterns, has long been part of a debate on whether one or the other type of carbon atoms (one with a carbon atom underneath and one without), or even hollow sites were imaged as bright spots. Although there is no such distinction between carbon atoms in single layer graphene, there is a substrate, which affects the local electronic structure at the atomic level. The uncertainty is removed only when the honeycomb pattern is observed. This is more likely to be obtained in Force/Force gradient images, and these parameters are more likely to reveal the topography of the surface compared to STM images. Hence, simultaneous STM/AFM operation is very useful in understanding the structure at the atomic scale. In our small amplitude simultaneous AFM/STM system, tip-surface distance was determined by tunnel current and STM topography was obtained. With the use of Lock-in Amplifier, the oscillation amplitude and phase shift in the desired frequency (far from resonance) were measured. In addition, by using the modulation in the tunnel current, the distance-derivative of the tunnel current, which is a measure of the tunnel barrier height, was also recorded using a second Lock-in Amplifier. High-resolution images of the graphene surface were obtained. These images were obtained using Si and W cantilevers. Atomic level resolution was obtained in all channels. In HOPG (Highly Oriented Prolytic Graphite) and two (or more) layers of graphene, there are three types of carbon atoms (*A*, *B* and *hollow*) due to the shifted settlements of layers with each other. Due to the dominance of electronic structure in STM images, mostly beta (*B*) atoms appear high. However, we show that the hollow sites can be observed in different imaging conditions. It is very difficult to determine such contrast differences on highly symmetrical and perfect surfaces such as graphite and graphene. Especially in STM topography and oscillation amplitude images, changes in the level of contrast caused by the changes in atomic structure of the tip were observed. In such simultaneous scans, there are a few pixels difference between the channels recorded directly from the control units and the channels from the lock-in amplifier. This depends on the selected measurement bandwidth of amplifier and scanning speed, which can also be calculated. In this study, we focused on the STM topography and the oscillation amplitude images, which is a measure of the force gradient. In the regions where the tip-surface distance is very small, we assume that because of the tunnel current saturation, the hollow sites in STM topography are displayed as brighter

points than *A* or *B* atoms. Based on the force-distance spectroscopy experiments, the scanning is performed in high repulsive force regime. In the results obtained with the Si cantilever, the brightest atoms in the STM images are supposed to be the beta (*B*) atoms. However, in some cases, the hollow sites or *A* and *hollow* sites were imaged as maxima points. Theoretical studies predicted this phenomenon when the tip-surface distance is very small. Furthermore, according to the interaction stiffness ( $k_{\text{int}}$ ) calculated from the oscillation amplitude images, the *hollow* sites have values greater than the *A* and *B* atoms. The results obtained with Si and W cantilevers are opposite where the carbon atoms reveal as maxima points in force gradient images rather than *hollow* sites. According to the previous theoretical calculations, most of these contrast types are explicable depending on imaging regime and tip type. The force and tunnel current spectroscopy curves show perfect agreement with the theoretical calculations reported by Ondráček et al.

In order to see the effect of tip trajectory in constant current scan on the contrast mechanisms of the force / force gradient images, experiments were carried out in constant height mode as well. The contrast in the oscillation amplitude (force gradient) images obtained at constant height mode does not show a big difference compared to that obtained in the constant current mode. The force gradient images obtained in these two different modes show similar contrasts.

Furthermore, we obtained different relative force gradient contrast between carbon atoms in an area as small as  $18 \times 18 \text{ \AA}^2$ . The results suggest a change in force contrast due to change in the interaction of the graphene layer with the underlying substrate. If the variation of graphene-substrate interaction is changing the electronic properties of graphene hugely, then uniform production of graphene in large scales becomes extremely important in order to obtain a uniform electronic structure.



## İKİ BOYUTLU MALZEMELERİN EŞZAMANLI ATOMİK KUVVET / TARAMALI TÜNELLEME MİKROSKOBU İLE İNCELENMESİ

### ÖZET

Bu çalışmada bakır folyo üzerine KBB yöntemi ile büyütülen grafen katmanlarının eş-zamanlı Atomik Kuvvet/Taramalı Tünelleme Mikroskopisi (AKM/TTM) ile incelenmesi ve elde edilen verilerin analizine ele alınmıştır. Bu incelemeleri çok küçük salınım genlikleriyle Ultra Yüksek Vakumda çalışan AKM/TTM ile gerçekleştirdik. Çok küçük salınım genliklerinin kullanılması, gerçeğe en yakın eş-zamanlı operasyonu mümkün kılmasının yanında, doğrudan ve nicel kuvvet/kuvvet gradiyeni ölçümleri yapmak açısından da gereklidir. Birkaç Ångstrom mertebesinde olduğu bilinen, ve atomik çözünürlükte görüntülemenin kaynağı olan kısa menzilli kuvvetlerin (kovalent bağlanma gibi) doğrudan ölçülmesi için düşük salınım genliklerinin (en azından Å-altı) kullanılması kaçınılmazdır. Ångström-altı genlikler kullanıldığında ölçülen genlik değişimi sinyalinden kuvvet/kuvvet gradiyeni bilgisini doğrudan elde etmek aşağıdaki işlem kadar kolaydır:

$$k_{int} = -\frac{dF}{dz} = k_{lever} \left( \frac{A_0}{A} - 1 \right)$$

Burada  $k_{int}$  etkileşim bükülmezliği,  $k_0$  yay sabiti,  $A_0$  ile  $A$  da sırasıyla etkileşim yokken ve varken salınım genlikleridir.

Küçük genlikli eş-zamanlı AKM/TTM sistemimizde uç-yüzey mesafesi tünel akımı ile kontrol edilip TTM topografisi elde edilirken, bir Kilitlemeli Yükseltici (Lock-in Amplifier) yardımıyla istenilen frekansta (rezonanstan uzak) salınım genliği ve faz kayması ölçülerek kuvvet gradiyeni ve enerji kaybı görüntüleri de elde edilmektedir. Bunun yanında tünel akımındaki modülasyonlardan yararlanılarak tünel bariyer yüksekliğinin bir ölçüsü olan tünel akımının mesafeye göre türevi de ikinci bir Kilitlemeli Yükseltici kullanılarak kaydedilebilmektedir. Değişik bilgiler içeren birçok niceliğin eş-zamanlı olarak ölçülmesiyle de örnek yüzeyi hakkında daha fazla bilgiye ulaşmak mümkün olmaktadır.

Grafen yüzeyinin eş-zamanlı AKM/TTM ile elde edilmiş yüksek çözünürlüklü görüntüleri elde edilmiştir. Bu görüntüler  $S_i$  ve  $W$  uç/yay kullanılarak elde edilmiştir. Taramalarda TTM topografisi, tünel akımı modülasyon genliği, yay salınım genliği ve faz kayması görüntülenmiştir. Tüm kanallarda atomik düzeyde çözünürlük elde edilmiştir. HOPG (Highly Oriented Prolytic Graphite) ve iki veya daha fazla katmandan oluşan grafen yüzeylerinde ardışık iki katmanın birbirine göre kaymış yerleşmesinden dolayı yüzeydeki atomların yarısının tam altında başka bir karbon atomu varken (alfa atomları), diğer yarısının altında boşluk vardır (beta atomları). Dolayısıyla yüzeydeki atomik yapılar alfa ve beta atomları ile boşluklardır. TTM görüntülerinde elektronik yapının baskınlığından dolayı çoğunlukla beta atomları yüksekte görünmektedir. Ancak değişik görüntüleme koşullarında boşlukların yüksekte gözlenebileceğini göstermekteyiz. Grafit ve grafen gibi çok simetrik ve

kusursuz yüzeylerde bu tür kontrast farklılıklarının belirlenmesi oldukça güçtür. AKM görüntülerinde ise farklı kuvvetlerin rol alabilmesi ve kuvvetin monotonik olmayan davranışından dolayı durum biraz daha komplike olabilmektedir. Taramalardan TTM topografisi dışında, tünel akımı modülasyon genliğinden tünel bariyer yüksekliği ve yay salınım genliğinden etkileşim bükülmezliği hesaplanmıştır. Özellikle TTM topografisi ve salınım genliği görüntülerinde yer yer iğnenin atomik yapısındaki değişimler kaynaklı kontrast seviyesi değişimi ve yapı farklılıkları gözlemlenmiştir. Bu tür eş zamanlı taramalarda doğrudan kontrol elektroniğinden okunan kanallar ile kilitlemeli yükselticiden okunan kanallar arasında birkaç piksel fark vardır. Bu kiltlemeli yükselticinin seçilen ölçüm bant aralığı ve tarama hızına bağlıdır ki, bu da hesaplanabilmektedir. Taramalarda salınım genliği ve tünel akımı modülasyon genliğindeki gecikme yaklaşık 6 pikseldir. Görüntülerde atomların yataydaki konumlarının iyi belirlenebilmesi için medyan filtremele gibi yöntemlerle filtrelenmişlerdir. Salınım genliği, faz kayması ve akım modülasyon genliği görüntülerinde parlak noktalar bu değerlerin daha yüksek olduğu yerlerdir. Bu çalışmada özellikle kuvvet gradyanının ölçüsü olan salınım genliği ve TTM topografisi görüntülerine odaklandık. Uç-yüzey mesafesinin çok küçük olduğu bölgelerde, muhtemelen tünel akımı yoğunluğundan dolayı TTM topografisinde boşluk atomları, A veya B atomundan daha parlak noktalar olarak görüntülediğini düşünüyoruz. TTM görüntüsünde uç-yüzey mesafesinin çok küçük olması ve olasılıkla uç yapısı kaynaklı bir distorsiyon olmakla birlikte karşılaştırma yapmaya olanak sağlanmıştır. Kuvvet-uzaklık spektroskopisi deneylerinde de görüleceği üzere oldukça yüksek itici kuvvetler bölgesinde çalışılmaktadır. Salınım genliğinin yüksek olduğu noktalar daha düşük itici kuvvete karşılık gelmektedir. Si uç/yay ile elde edilen sonuçlarda TTM görüntüsündeki parlak atomların -genel kabule göre- beta (B) atomları olduğunu kabul edersek salınım genliğindeki (etkileşim bükülmezliğinin tersi) daha parlak görünen noktalar alfa (A) atomlarıdır. Ayrıca salınım genliği görüntüsünden hesaplanan etkileşim bükülmezliği ( $k_{int}$ ) göre boşluk atomu A ve B atomlarından daha büyük değerlere sahiptir. İlk bakışta, A ve B atomları yaklaşık aynı olmak üzere, boşluklardan daha yüksek bir  $k_{int}$  değeri vermeleri düşünülür. Çünkü bu atomlar uca daha yakındırlar. Ancak, bundan önceki teorik çalışmalarda da belirtildiği gibi, uçun yapısı ve reaktivitesi Kuvvet etkileşiminde önemli bir role oynamaktadır. Si ve W uç/yay ile elde ettiğimiz sonuçlar tam tersidir. Sabit tünel akımı kipinde uç buna göre bir yol takip ettiğinden, bu yolun korüstasyonuna bağlı olarak, belli bir noktada ölçülen etkileşim, sadece o noktadaki atomla değil, o atomun etrafındaki atomlardan da kaynaklana bileceği düşünülmüştür. Ucun bu doğrusal olmayan yolunun etkisini görmek amacıyla, özellikle kuvvet/kuvvet türevi görüntülerindeki kontrast mekanizmalarına ışık tutabileceğini düşündüğümüz sabit yükseklik kipinde görüntüleme deneyleri de yapılmıştır. Sabit yükseklikte elde edilen salınım genliği (kuvvet türevi) görüntüsündeki kontrastta sabit tünel akımında elde edilene kıyasen büyük bir fark görülmemektedir. Bu iki farklı modda elde edilen kuvvet türevi görüntülerinin birbirlerine benzer kontrast vermeleri göstermiştir ki; Ucun sabit tünel akımı kipinde takip ettiği yol kuvvet türevi görüntüsündeki kontrastta büyük etkisi yoktur.

Özellikle W uç/yay ile elde edilmiş eş-zamanlı AKM/TTM taramalarda tüm ayarlamalı parametrelerde etkileşim bükülmezliği görüntülerinde balpeteği yapısı görünmektedir. TTM'deki parlak noktaların, yüzeye olan mesafe göz önünde bulunarak, boşluk ve B atomları olduğu tesbit edilmiştir. Görüntülemeledeki kontrast farklılıklarına ışık tutması ve atomlararası kuvvet/kuvvet türevi gibi etkileşimleri ölçmek amacıyla Kuvvet-uzaklık (F-d) spektroskopisi diye adlandırdığımız ölçümler

de yapılmıştır. Örnek üzerinde belli bir noktada yüzey ile uç arasındaki mesafeyi değiştirirken kuvvet/kuvvet türevinin yanı sıra yine eş-zamanlı olarak tünel akımı, tünel bariyer yüksekliği gibi nicelikleri ölçtüğümüz bu yöntemle de bu niceliklerin mesafe ile ve birbirleriyle olan ilişkilerini belirleyebilmekteyiz. Grafen yüzeyinde Si ve W uç/yay ile bu ölçümler elde yapılmıştır. Bu eğriler kendi başlarına ele alındığında kabaca beklenen davranışları sergilemişlerdir. Tünel akımı (burada logaritmik eksenslidir) mesafeye üstel bağlı değişim göstermiş, kuvvet beklendiği gibi önce çekici bölgede artıp maksimuma ulaştıktan sonra sıfıra dönüp itici bölgede artışına devam etmiştir. Ancak tünel akımı ve kuvvet etkileşimlerinin menzillerini karşılaştırdığımızda incelediğimiz başka birçok örneğe göre farklı bir durum görmekteyiz. Daha önceki benzeri çalışmalarda incelenen Si(111), Si(100) gibi yarıiletken ve Cu(100) gibi metal yüzeylerinde akım ve kuvvet türevi etkileşimlerinin yaklaşık olarak aynı mesafelerde başladığı gözlenmiştir. Bu da TTM'de kullanılan tipik tünel akımı değerlerinde kuvvetin çekici bölgesinde çalışmayı olanaklı kılmıştır. Grafen yüzeyindeki ölçümlerimizde durum çok farklıdır. Etkileşim bükülmezliği ve kuvvet etkileşimi tünel akımından çok daha uzak mesafelerde başlamaktadır. Eş-zamanlı AKM/TTM sistemimizde mesafe kontrolünü tünel akımı üzerinden sağladığımız için 0.1-0.2 nA gibi mütevazı akım değerlerinde bile uç itici kuvvet bölgesinde bulunmaktadır. Bu da örnek yüzey kuvvet etkileşiminin çok yüksek olması dolayısıyla görüntülemeyi zorlaştırmaktadır. Daha da önemlisi sadece TTM operasyonunda bile uç ve yüzey atomlarının ne kadar büyük kuvvetlere maruz kaldıkları ve bunların etkisiyle görüntüleme sırasında yer değiştirebileceklerini göstermektedir. TTM'nin icadından sonraki ilk yıllardan itibaren ileri sürülen, kuvvetin rolüne dair bu tür yorumlar ve teorik hesaplamalar, grafen yüzeyindeki deneylerimizde bir kez daha desteklenmiş olmaktadır.

Yukarıdaki çalışmalara ek olarak, KBB yöntemi ile bakır üzerinde büyütülmüş grafenin, PMMA yöntemi ile SiO<sub>2</sub> levha üzerine aktarıldıktan sonra, levha yüzeyindeki grafenden bağlantı alınıp eş zamanlı AKM/TTM ile incelemeleri yapılmıştır. Bu çalışmayla, bakır alttaşının grafen yüzeyi incelemelerindeki etkisini araştırmak amaçlanmıştır. Bakır alttaşının grafen yüzeyi incelemelerinde iki temel etkisi olabileceği tartışılmaktadır. Birincisi, grafen tabakasıyla alttaki bakır kristal yapısının uyumsuz yerleşmesinden kaynaklanan Moire deseni gibi sonuçların ortaya çıkabileceğidir. İkincisi ise, bakırın yüksek elektron yoğunluğunun grafen tabakasının yerel durum yoğunluğunu (LDOS) etkilemesi ve ayrıca AKM/TTM nin tüm kanallarında gözardı edilemez bir etkileşime yol açmasıdır. SiO<sub>2</sub> üzeri grafen yüzeyinin eşzamanlı AKM/TTM incelemelerinin sonuçlarında, TTM topografi ve tünel akımı modülasyon genliği kanallarında atomic çözünürlük elde edilirken, salınım genliği kanalında (kuvvet türevi) atomik yapılar gözlemlenememiştir. Bunun nedeni, tarama sırasında azalan sinyal gürültü oranıdır. TTM topografi ve tünel akımı modülasyon genliği (tünel bariyer yüksekliği) kanallarında, bakır üstü grafen incelemelerine benzer bir şekilde grafen tabakanın altıgen (peteğimsi) yapısındaki altı karbon atomundan üç tanesi (B atomları) diğer üçüne (A atomları) nispeten yüksek görünmektedir. Dolayısıyla, incelemelerimizde ki A ve B atomlarının farklı yükseklikte görüntülenmelerinin en muhtemel nedeni, üstüste büyütülmüş iki grafen tabakasının kaymış yerleşmesidir.

Ayrıca, bir başka iki boyutlu malzeme Bi<sub>2</sub>Te<sub>3</sub> yüzeyinde eşzamanlı TTM/AKM ile görüntüleme yapılmıştır. Bi<sub>2</sub>Te<sub>3</sub> örneği, sentetik olarak üretilmiş Bi<sub>2</sub>Te<sub>3</sub> peletin yüzeyinden katman ayırmak suretiyle görüntülemeye hazır hale getirilir. TTM

Topografisi, Tünel akımı modülasyon genliđi ve salınım genliđi kanallarında atomik düzeyde çözünürlük elde edilmiştir.



## 1. INTRODUCTION

Two-dimensional materials, particularly Graphene, are among most promising materials for use in future nanotechnology due to novel mechanical and electronic characteristics. Graphene is a two-dimensional honeycomb lattice of  $sp^2$  carbon atoms that has attracted intense attention of researchers mostly because of its unique electronic properties, such as giant charge carrier mobility [1] and strange quantum Hall effect [2], which originates from massless Dirac fermions with linear energy dispersion in the electronic band structure [3].

Besides these inherent electronic properties which has been theoretically anticipated, the specific characterization of graphene in atomic scale using high sensitive Scanning Probe Microscopes (SPM) such as high resolution Atomic Force Microscopy (AFM) and Scanning Tunnelin Microscopy (STM) would be very useful. Based on the variety of studies, STM and AFM images of Graphene can be seen as Moiré, Honeycomb or Trigonal patterns depending on different experimental parameters. The most effective parameters in STM and AFM results can be summarized as the tip type, distance range of interaction during operation of microscope, applied bias voltage and bond strength of underlying substrate as well as its lattice type. Some of these results and related conditions of experiments will be summarized here to help us better understand and interpret of our rarely seen results, acquired by our specially designed simultaneous AFM/STM.

Moiré pattern has been seen in both STM and AFM investigations. The most reliable interpretations for imaging this pattern are classified as shift of successive layers of Graphene and lattice-mismatched between Graphene and underlying metallic substrate. In Highly Oriented Pyrolytic Graphite (HOPG) and multilayer graphene, due to the shift between two successive layers, three carbon atoms have direct neighbor at the below graphene layer that defined as A ( $\alpha$ ) atoms and other three carbon atoms get place right above the hollow sites of the underlying Graphene layer which defined as B ( $\beta$ ) atoms, makes these two type of surface atoms inequivalent. Since, B atoms have greater contribution to the density of state close to Fermi Energy compared to A

atoms, are imaged as bright spots at relatively low bias voltages based on the STM investigations. However, during past decades Trigonal patterns were reported for a broad range of bias voltages [4-6], in addition, some groups have reported honeycomb pattern even for low biases [6-10].

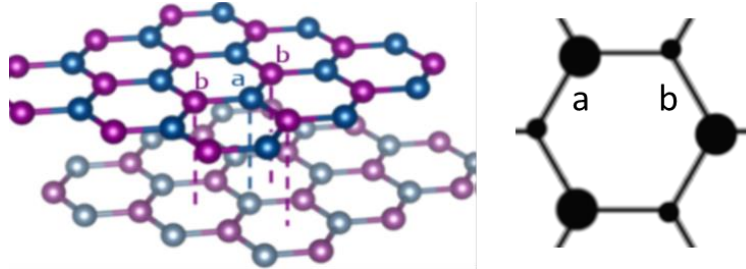


**Figure 1.1** : Schematics of bilayer graphene and a unit cell.

Graphene-metal bond could be subdivided into two main groups of “strongly bonded” and “weakly bonded”. Where Graphene-Ni, Graphene-Co and Graphene-Rh are classified as strongly bonded and some others such as Graphene-Cu, Graphene-Au and Graphene-Ir taken place in weakly bonded group. Moreover, Graphene-Metal interaction can be resulted as lattice-matched (Graphene-3d Metals) or lattice-mismatched (Graphene-4d, 5d Metals).

Where honeycomb pattern images are interpreting as imaging of all six carbon atoms, the Trigonal pattern of bright spots are evaluating as imaging of 3 of 6 carbon atoms (A or B) or not each of them but Hollow sites. Despite numerous investigations and the simplicity of honeycomb structure of graphene, interpreting the maxima points in scanning probe microscopy images as atoms or hollow sites is a fundamental challenging problem yet [11-14].

Theoretically, current in scanning tunneling microscopy (STM) and attractive force in atomic force microscopy (AFM) have the same origin [15]. While repulsive force is directly shaped the protrusions (atoms) in the topography image during operation of AFM in very close distances to the surface (repulsive regime) because of Pauli’s exclusion law. STM behavior is more complicated where it could be interpreted as map of the charge density of surface so depend on tip type and its charge state; maxima points in the topography image could be corresponded to the hollow sites or each of the atom types with different charge states.

## 1.1 Purpose of Thesis

Graphene has been one of the most encouraging materials for upcoming electronic devices. Actually, there are distinct advancements in the areas of electronic transport where this material outperforms: An outstanding conductivity at room temperature. Due to these unique properties, graphene was one of the most attractive material for investigation by Scanning Probe Microscopies. However, the contrast of STM images was the subject of debate among researchers for many years where three carbon atoms of hexagonal structure of graphene were not imaged by this technique. Scanning with AFM was the only way to extract the surface topography. Electronic characteristics of graphene and interaction with substrate dominantly were affected in STM measurements that makes doubts about electronic structure of graphene and the effect of interaction with subsurface atoms in the resulting measurements. Having the possibility to make measurements both by STM and AFM at the same time and same area could be best way to avoid the doubts. Investigation of mechanical and electronic properties of 2D materials such as graphene using our high resolution simultaneous AFM/STM would be very useful for this demand. The use of simultaneous AFM/STM may shed light on the contrast mechanisms in SPM of graphene. Our high sensitive home-built microscope with the use of very small oscillation amplitudes allows us to perform true simultaneous AFM/STM. Studying graphene surface at the atomic scale, using Si and W tips, and different experimental parameters would contribute to the existing literature on SPM –particularly STM- of graphene and HOPG. This would in turn contribute to the advancement in science and technology related to 2D materials.

## 1.2 Literature Review

### 1.2.1 Highly oriented pyrolytic graphite (HOPG)

Highly oriented pyrolytic graphite (HOPG) is a widely used sample in studies conducted with scanning probe microscopy (SPM) because of its atomically flat surface that can be simply cleaved and due to the fact that atomic resolution can be regularly acquired in ambient and vacuum conditions. HOPG is made up by planar  $sp^2$  bonds where the length of C–C bond is about 1.42 Å. Planes are kept together by van der Waals force. The graphene layers in HOPG are slidable due to this weak van der Waals force. Along the c-axis of the HOPG crystal, the graphene layers pile in ABAB arrangement. Carbon atoms of top graphene layer are divided in two groups known as; A ( $\alpha$ ) atoms and B ( $\beta$ ) atoms [16]. A ( $\alpha$ ) atoms locate atop the carbon atoms and B ( $\beta$ ) atoms take place right on the hollow sites of the underlying graphene, as shown in (Figure 1.2.a). There is a strong asymmetry of the local density of states (LDOS) between the two types of carbon atoms in the topmost graphene layer, which was shown by band structure calculations at the Fermi level [17]. B atoms are more detectable by STM owing to the LDOS near the Fermi level which is higher than that of the A atoms. These B atoms shaped a new bigger triangular structure in STM images (two lattice points in this triangular structure spaced  $\sqrt{3}$  times the typical neighboring C–C bond length, It means a unit cell length of about 0.246 nm).

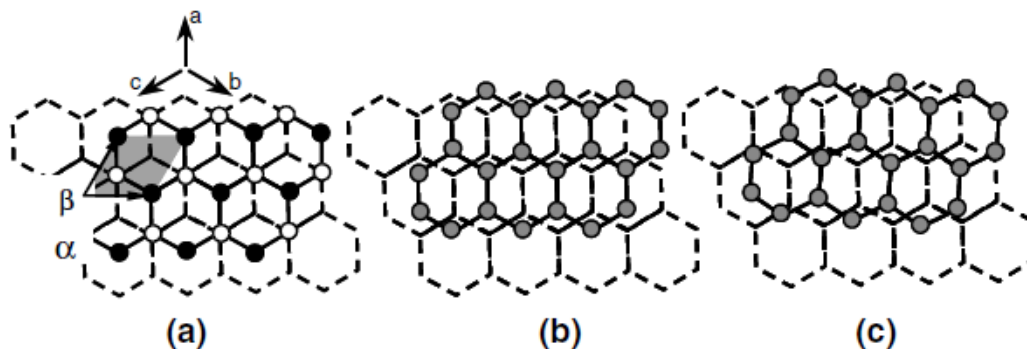


**Figure 1.2 :** Schematic of two layers of HOPG. (a) Normal stacking where A atoms and B atoms are indicated by open circles and solid circles respectively. (b) Top layer was shifted without rotation. (c) Top layer was shifted with a rotation. In this situation, the Moiré' pattern can be seen in STM topography, taken from ref. [10].



The fact that  $\alpha$  and  $\beta$  atoms have different LDOS clarifies why the STM images of HOPG exhibited the triangular structure rather than the uniform honeycomb structure of graphene. Consequently, only three carbon atoms can be often imaged by STM and there are three invisible carbon atoms in the obtained topography. Researchers have been trying to observe the three hidden carbon atoms. S. Hembacher, F. Giessibl et al. acquired proper results in observing the three hidden atoms particularly in AFM images at low temperature (4.89 K) using the STM/AFM setup they developed. However, all six carbon atoms could not be seen with STM at such a low temperature. Investigation of Graphite with FM-AFM/STM in low temperature using a metallic tip (W) attached to a tuning fork with stiffness of ( $k=2000$  N/m) and relatively small amplitudes ( $A=5$  Å), which enables simultaneous imaging of tunneling current and frequency shift, shows that trigonal and honeycomb pattern can be seen as a function of distance and bias voltages from attractive to repulsive regime [12].

Furthermore, big hexagonal periodic patterns, known as Moire' patterns, have been observed with periodicities in the range of several nm, which were promptly ended by sharp boundaries [18–21]. These periodic Moire' patterns were generally referred to rotational misorientation of layers, double tip effect, lattice mismatch or defect masked deep in subsurfaces.

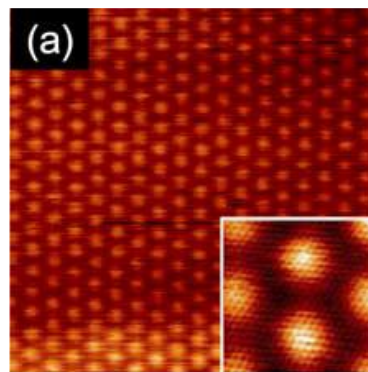


**Figure 1.3 :** Typical STM image of Moire' pattern on HOPG surface (50 nm × 50 nm) and an enlarged zone (6 nm x 6 nm), taken from ref. [10].

### 1.2.2 Graphene

Carbon atoms, which are attached together in a firmly two-dimensional structure, shape a graphene sheet, where each atom has three in-plane neighbors, yielding a honeycomb mesh. Besides, graphene layers are classified as weakly bonded two-

dimensional materials that can be easily slide on each other. A. Geim and K. Novoselov made use of this idea in order to produce graphene, which caused to demonstration of its unique electronic properties, i.e. the photon-like behavior of the charge carriers, and brought them the Nobel Prize in physics in 2010.

Graphene, a single layer of carbon, shows some fascinating characteristics. In particular, it has the largest tensile strength ever measured. In contrast to this great internal strength, Graphene bounds weakly to outside world, particularly to metal surfaces on which it can be produced by epitaxial growth [22, 23].

During the last decades, graphene was subject of many studies using STM and AFM. While STM images generally shows trigonal pattern with bright spots corresponded to B atoms, the AFM images in fully repulsive regime shows honeycomb pattern that claimed as imaging of all six atoms [12]. The use of Si cantilevers is common in Atomic Force Microscopy (AFM). However, Si cantilevers are classified as weakly reactive tips. The dominant force in tip-graphene interaction is repulsive and belongs to Pauli repulsion exclusion and bright spots in AFM images are interpreted as hollow sites [11]. Some FM-AFM studies on Graphite (0001) show a triagonal pattern of bright spots instead of honeycomb in agreement with this description [24]. On the other hand, metallic tips are classified as reactive tips where due to the strong interaction between tip and carbon atoms, atomic resolution contrast can be obtained in both attractive and repulsive regimes however with inverted contrast. Ondráček et al. reported a theoretical study demonstrating the force behavior of different tip types on the carbon atoms and hollow sites [25]. Some of their calculated results are shown in figure 1.4. These results show that the atomic contrast on the carbon surfaces in the AFM is highly dependent on the tip reactivity. Beyond the force maximum, the interaction force is more attractive on hollow sites compared to carbon atoms by using metal tips particularly W and Ir, whereas in the case of Si tip, reverse behavior can be observed. This strange behavior can be seen more dominantly with the use of H3 Si tip.

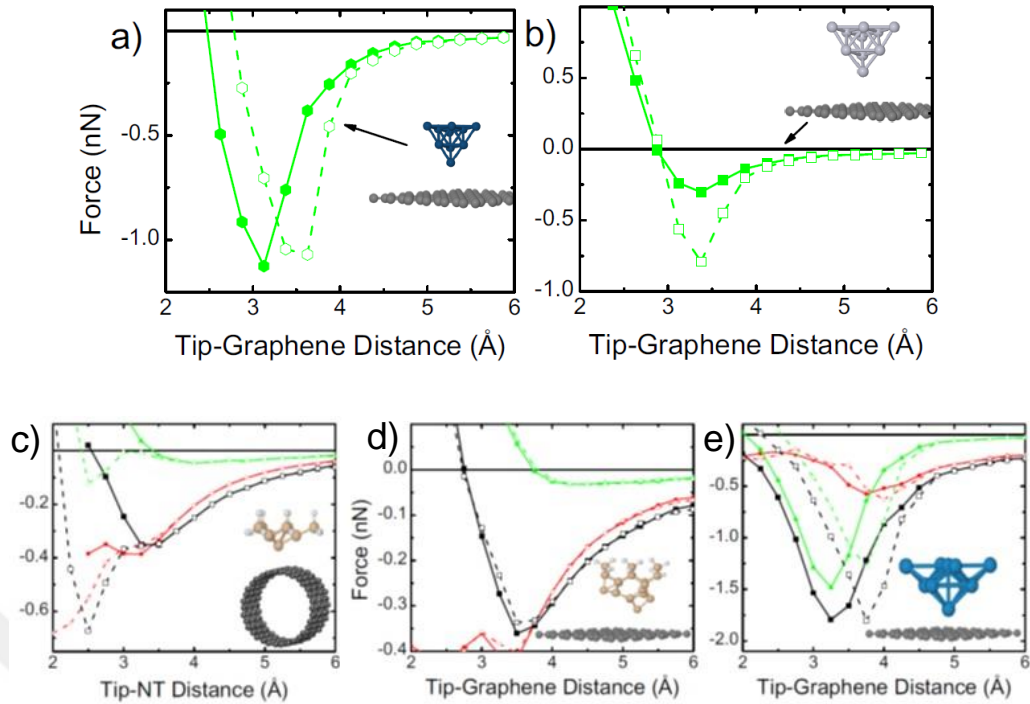


**Figure 1.4 :** Force as function of tip-surface distance are calculated on carbon atoms (open symbols) and hollow sites (solid symbols) for a) Ir b) Pt c) H3 Si d) dimer terminated Si and e) W tips, taken from ref. [25].

Epitaxial growth of Graphene on metal surfaces is more adopted for technological production, generating large, well-ordered films [22]. In addition, Graphene monolayers can be grown on metallic surfaces, mostly through thermal decomposition of hydrocarbons or surface segregation of carbon atoms from the bulk metal. Accordingly, graphene has been grown onto Co (0001) [26], Ni (111) [27], Pt (111) [28-30], Pd (111) [31], Ru (0001) [32] or Ir (111) [33-35].

Graphene indicates strong internal bonding, but only weak interaction with metal substrate. Therefore, it is essential to figure out whether the attendance of the metal substrate disrupts the specific properties of graphene, and whether it is possible to keep away graphene from further processing. In both cases, the strength of the binding between graphene and substrate plays main role. Simultaneous FM-AFM/STM imaging of Graphene on Ir substrate in room temperature during operating in attractive regime shows three atoms brighter than other three atoms in AFM image, which interpreted as influence of van der Waals forces, belong to underlying Ir atoms. But, in STM image, the hollow sites were imaged as bright spots due to the dominance of electronic density of states of underlying Ir (111) atoms [18, 36].

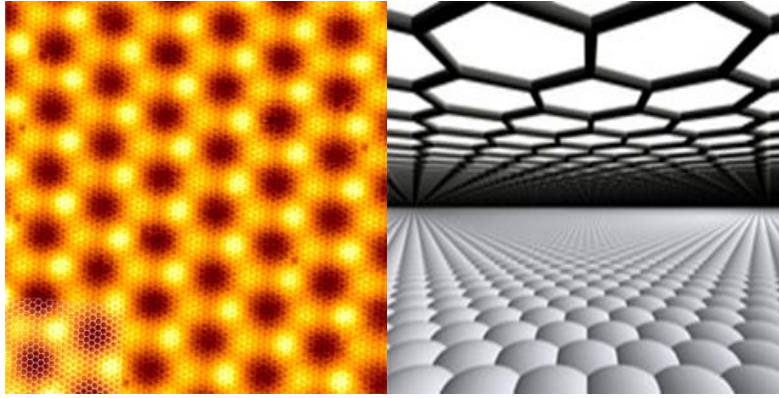


**Figure 1.5 :** STM image of graphene on Ir (111). The moiré patterns result from the superposition of the graphene lattice with the lattice of the underlying metal surface. The image size is 15 nm × 15 nm, taken from ref. [22].

The zigzag and armchair are two types of structure that are observed in graphene edges. The edge geometry has significant effect on the electronic structure of graphene sheet.

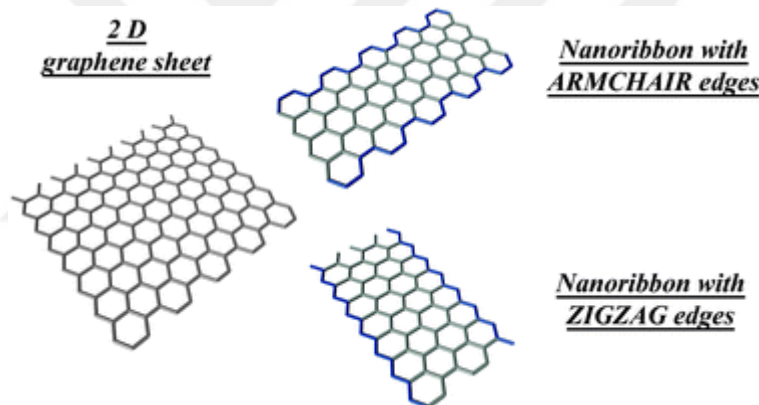


**Figure 1.6 :** Drawing schematics of the edge structures in graphene sheet and nanoribbon. (Image courtesy of M. Hofmann, MIT).

The zigzag edge consists of the nonbonding p-electron state, which can not be seen, in the armchair edge. For example, the graphene nanoribbon, which ends by zigzag edges on both sides, has been proposed to have a distinct localized state at the edge [37]. The localized spins at the edge emerge as incomparable magnetic properties [38, 49].

These specific magnetic properties of zigzag-edged nanosized graphene with unique shapes, such as triangular and hexagonal, have been demonstrated by theoretical studies [40, 41].

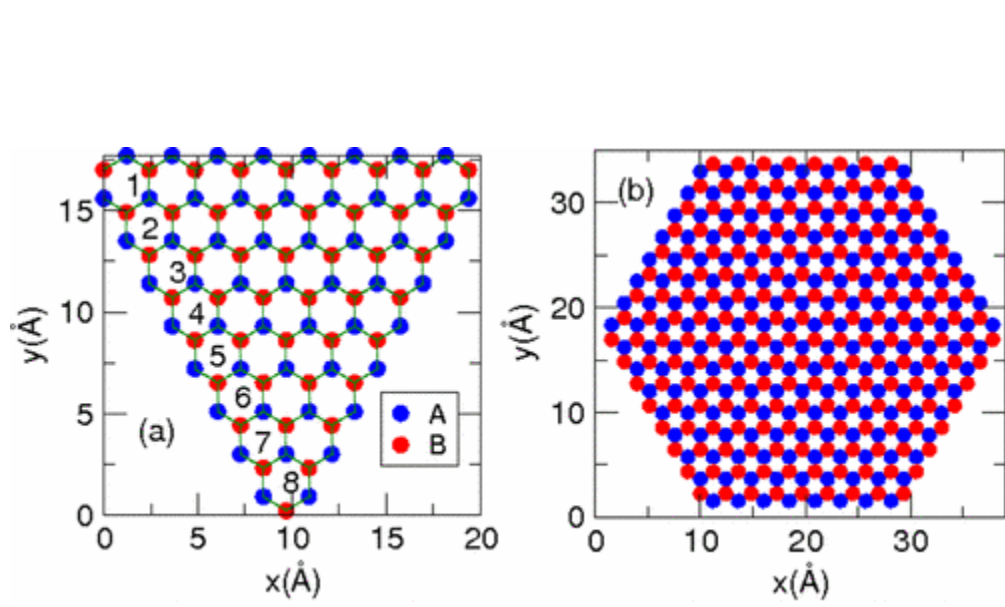


**Figure 1.7 :** Triangular and hexagonal shapes of zigzag edges are formed by atoms that belong to the same sublattice, A or B type, taken from ref. [40]





## 2. METHODS AND EQUIPMENTS

### 2.1 Scanning Tunneling Microscopy

A scanning tunneling microscope (STM) is an instrument for imaging surfaces at the atomic scale which was developed in 1981 by Gerd Binnig and Heinrich Rohrer (at IBM Zürich) and earned its inventors the Nobel Prize in Physics in 1986. This instrument is working based on the concept of quantum tunneling. The quantum tunneling is among the well-known quantum mechanical principals that consider the possibility of electron passing through a potential barrier. At this concept, in a specific distance between tip and sample and by applying the bias voltage, the current flow can be obtained due to the difference in the energy state of tip and sample as shown in figure 2.1.

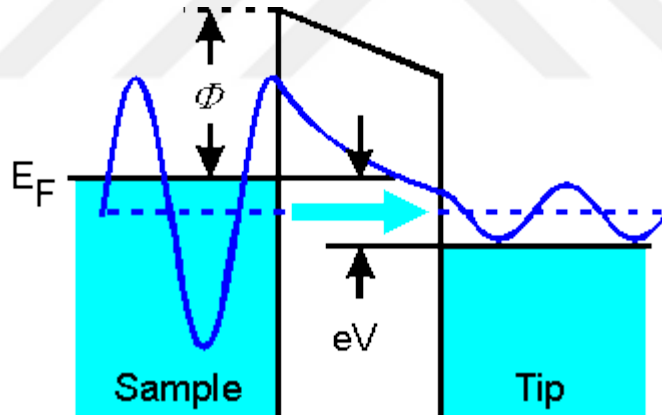


**Figure 2.1 :** Drawing schematic of the quantum tunneling in STM setup.

This electron flow is called tunnel current, which depends on the applied bias voltage, tip-sample distance and surface local density. The calculated relation as a solution of Schrödinger equation is given by equation 2.1 as;

$$I \approx \sum_{E_F - eV}^{E_F} |\Psi_n(0)|^2 e^{-2kz} \approx V \rho_s(0, E_F) e^{-2kz} \quad (2.1)$$

Where  $K$  is the decay constant and can be derived as a function of work function ( $\phi$ ) is given by equation 2.2 as;

$$K = 0.51\sqrt{\phi(eV)} \quad (2.2)$$

The STM setup as displayed in figure 2.2, includes tip, sample, coarse positioner, scanning piezo and I-V converter. The tunnel current is set to a desired value to approach the tip towards the surface and then surface can be scanned by using the set tunnel current as feedback control parameter. The topography of surface is mapped as a result. Scanning tunneling microscopy has two main modes known as constant current and constant height. As mentioned, scanning of the surface using tunnel current as feedback is called constant current scan mode while scanning the surface in constant height mode is fulfilled by keeping the tip in constant height during the scan without using feedback loop. The former one gives the surface topography, whereas the latter provides a map of tunnel current change. The variation of tunnel current during constant height scan depends on the change of the local density of states as well as surface morphology.

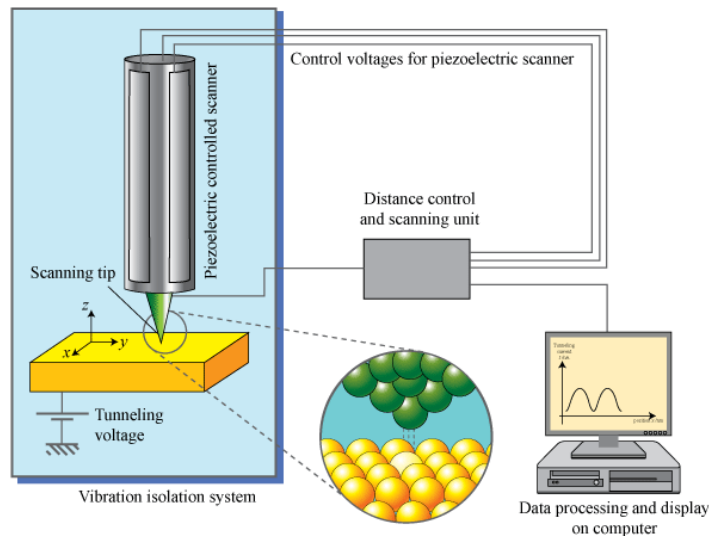


**Figure 2.2 :** Drawing schematic of typical STM setup.

## 2.2 Atomic Force Microscopy

Since the Scanning Tunneling Microscopy (STM) is limited to scan the conducting and semi-conducting surfaces, the need for an instrument with the ability to image topography of surface for both conductive and non-conductive samples was the main motivation to invent the Atomic Force Microscope (AFM).



In 1985, Binnig, Quate, and Gerber invented another setup in the family of scanning probe microscopes, which works based on the interatomic force between the tip and sample and enables to image topography of surface for both conductive and non-conductive samples. This instrument was named Atomic Force Microscopy (AFM). Topography imaging did not satisfy scientists who needed more quantitative measurements for material characterizations. Thus, various imaging modes were evolved for quantitative measurements on the samples. Traditionally, a laser beam and photodetector are used in deflection detection setup of most of atomic force microscopes as displayed in figure 2.3, where the reflected laser beam from the back of the cantilever reaches to the position detector, which consists of four quadrants. Consequently, the cantilever's vertical and horizontal movements could be detected which leads to extract the normal and lateral forces.

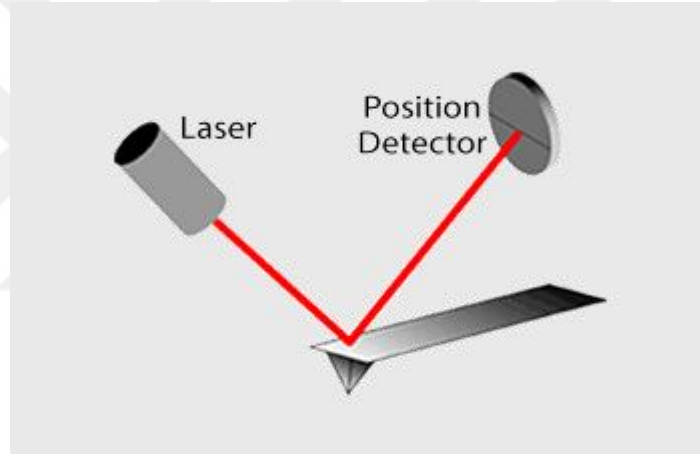


**Figure 2.3 :** Drawing schematic of typical AFM setup.

The Lennard-Jones potential between two particular atoms is given by equation 2.3, which depends on the distance ( $R$ ) between them. This term of potential energy consists of two long range (van der Waals) and short range (ionic) interactions.

$$U(R) = 4\epsilon \left[ \left( \frac{\sigma}{R} \right)^{12} - \left( \frac{\sigma}{R} \right)^6 \right] \quad (2.3)$$

Where  $\epsilon$  and  $\sigma$  are the potential well depth and the distance where the potential equals zero, respectively. The force between two atoms can be derived by equation 2.4 as;

$$F = - \frac{dU}{dR} \quad (2.4)$$

The behavior of the force interaction between two atoms depending on the distance between them is shown in figure 2.4.

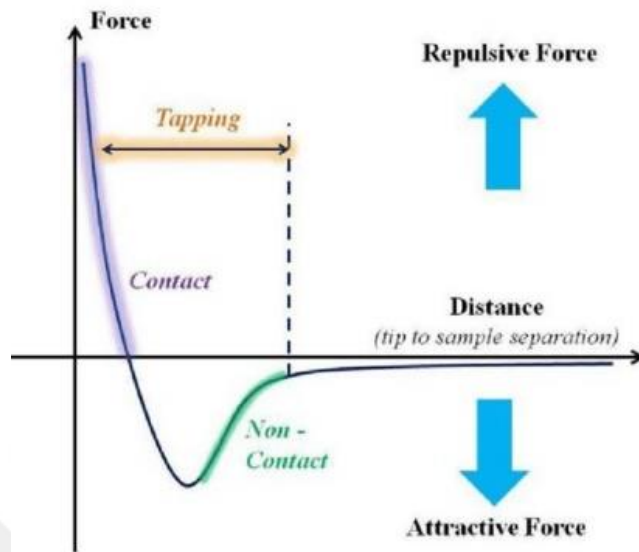


**Figure 2.4 :** Typical Force-Distance curve between two atoms and indicated operating regimes in different AFM modes.

Atomic force microscopy has two main modes known as contact and dynamic modes. During the scan of surface in contact mode, because of the direct interaction of tip and surface the surface topography can be obtained by using the bending of cantilever (constant force) as a feedback loop. The dynamic mode is also divided into two different modes named noncontact and tapping modes. In both of these modes the cantilever is oscillated at the resonance frequency. The behavior of amplitude and resonance frequency of the cantilever depends on the tip-sample interaction, as displayed in figure 2.5. In the tapping mode, the amplitude of the cantilever is kept constant during the scan of the surface, while in the noncontact mode the frequency shift due to the tip-surface interaction is taken as a constant value to acquire the surface topography.

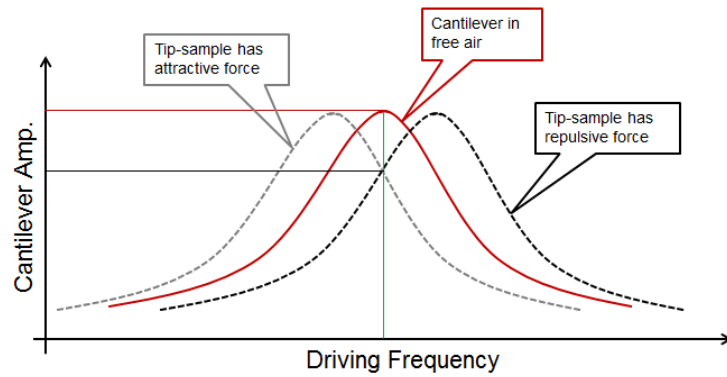


**Figure 2.5 :** Resonance frequency shift of cantilever during the interaction with sample in the attractive and repulsive force regimes.

### 2.3 Simultaneous STM/AFM

The invention of scanning tunneling microscopy STM and atomic force microscopy AFM opened completely new perspective in characterization and imaging of surfaces and nanostructures in atomic scale. In STM, the tunneling current between a probe and sample is used as feedback loop to surface scanning. It became widely used due to its simple design compared to AFM. However, tunneling current to be the measured signal restricts STM to conducting and semi-conducting surfaces only. This limitation was overcome by the invention of AFM, which senses atomic forces acting between foremost atoms of probe and sample.

The combination of these two techniques attracts great attention for conducting or semiconducting samples, because the acquired spectroscopies associated to forces and tunneling current between foremost atoms of probe and sample provide complementary results. It would be helpful to detect distinct unique structures or chemical adsorbates on surfaces or in nanostructures.

Oscillation amplitude of cantilever plays a major role for actually simultaneous measurement of forces and tunneling current. Large lever oscillation amplitudes comprises a limited range in which tip is in tunneling cycle, so time and separation averaged current is measured. Consequently, making simultaneous STM and AFM requires very small lever oscillation amplitudes. Using sub-angstrom oscillation amplitudes allows to operate Simultaneous STM/AFM system as close as possible to true STM mode [42, 43].

The head of our home-built simultaneous AFM/STM is displayed in figure 2.6. This system with sensitivity of  $2 \times 10^{-4} \text{ \AA}/\sqrt{\text{Hz}}$  is capable of measuring the force gradient interactions between the tip and the sample as well as tunnel current, work function (tunnel barrier height), and energy dissipation [44,45].

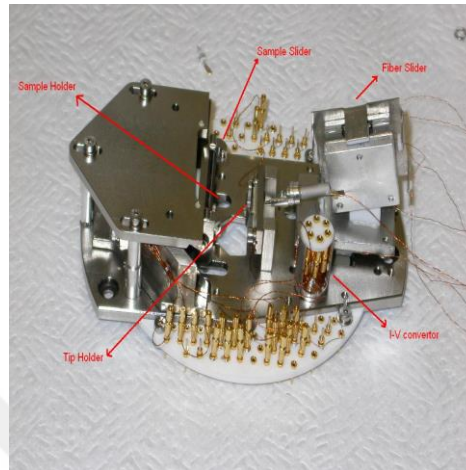


**Figure 2.6 :** Head of home-built simultaneous AFM/STM.

### 2.3.1 Fiber optic interferometer setup

Our system is a commercial Ultra High Vacuum Scanning Probe Microscope that was modified and improved using a Fabry-Perot fiber interferometer to achieve high sensitivity to lever deflection, which in turn allows us to conduct simultaneous STM/AFM measurements [42, 45].

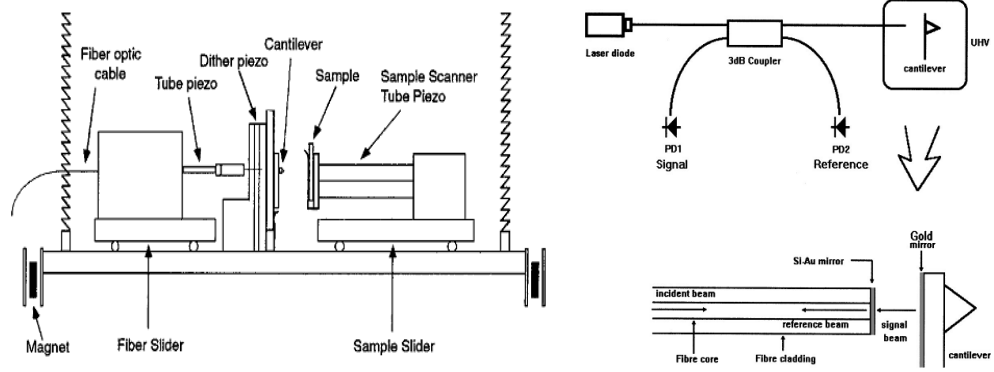


**Figure 2.7 :** Schematics of AFM/STM microscope and Fabry-Perot fiber interferometer, taken from ref. [42].

The fiber interferometer, as shown in figure 2.7, consists of a cleaved and Silicon-Gold coated fiber with total reflectivity of 45%, a single mode laser diode operated at constant power and 50% fiber splitter as shown in Fig. 6. One of the outputs of splitter is connected to the fiber, which is positioned very close to the back of cantilever into the UHV system and the other output and the input of the splitter are connected to reference and signal photodiodes, respectively. Two reflected beams from the end of coated fiber and back of cantilever reach to the signal photodiode and their Interference generates a photocurrent at the signal photodiode. If the fiber is located parallel and very close to the lever, a Fabry-Perot cavity is formed and the signal photodiode current can be written by equation 2.5 as:

$$i = i_0 \left[ 1 - VF \left( \frac{4\pi d}{\lambda} \right) \right] \quad (2.5)$$

Where  $V$ ,  $d$  and  $\lambda$  are visibility, fiber-lever separation, and the wavelength of the laser and  $F(d)$  is a periodic function of  $d$ . At the quadrature points,  $d = \lambda/8, 3\lambda/8, 5\lambda/8, \dots$ , the interferometer is at the most sensitive position. The slope of this function  $F'(d) = m$ , is always greater than one at the proper quadrature point in which the smallest displacement that can be measured by our interferometer [42]. A typical interference pattern obtained by using W cantilever is shown in figure 2.8. The maximum slope in this pattern is the most sensitive point for measuring the cantilever displacement. By locking the fiber at this point, the oscillation amplitude in sub-angstrom level can be recorded.

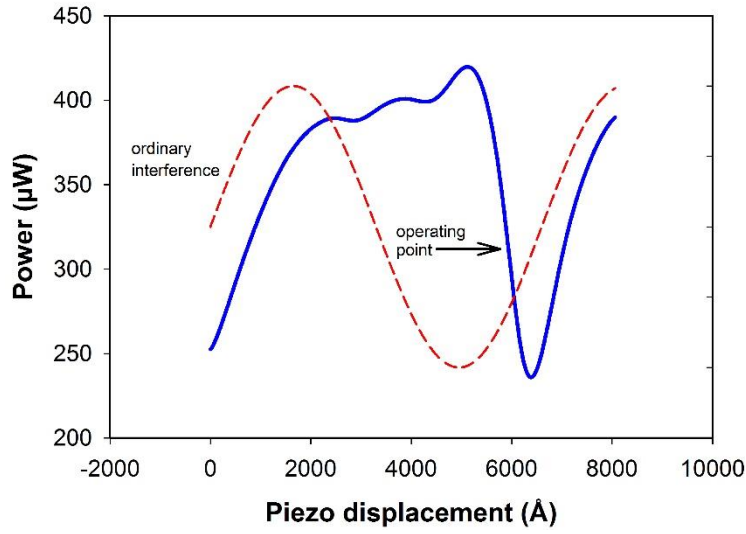


**Figure 2.8 :** Typical interference pattern obtained with W cantilever. The most sensitive point is indicated by arrow with the maximum slope of  $(-107.98 \text{ mV}/\text{Å})$ .

Using a RF modulation in the scale of few hundred MHz in dc input of the laser driver, causes to enhancement in signal to noise level by overwhelming the problematic power fluctuations of laser diode [42].

### 2.3.2 Calibration of cantilever

In investigation of materials by AFM, besides high-resolution imaging, the extracting actual characteristics of materials and related quantities is more significant. For this reason, the true calibration of cantilever plays a key role to pull out more veritable mechanical characteristics of materials. The most important properties of cantilever, which is essentially required to be extracted, are the stiffness and resonance frequency. Different methods were introduced for the calibration of cantilever. The most primitive of them is based on the physical dimension of cantilever. Using the dimensions of cantilever and Young's modulus, the stiffness of cantilever can be derived by equation as;

$$K = \frac{Ewt^3}{4l^3} \quad (2.6)$$

Where  $w, t$  and  $l$  are width, thickness and length of cantilever respectively. The need for more precise calibration caused to develop new techniques. One of these techniques is based on the equipartition theorem of energy using thermal excitation.

The relationship between thermal and kinetic energies of cantilever is given by equation 2.7 as;

$$\frac{1}{2}K \langle z^2 \rangle = \frac{1}{2}K_B T \quad (2.7)$$

In the recent years, Fukuma has made progress on this method using the equation 2.8, introduced by Albrecht et al. and named as thermal Brownian noise, which is in good agreement with experimental results [46].

$$n_{ZB} = \sqrt{\frac{2K_B T}{\pi \omega_0 K Q [1 - (\omega/\omega_0)^2]^2 + [\omega/(\omega_0 Q)]^2}} \quad (2.8)$$

Where  $K_B$ ,  $T$ ,  $\omega_0$  and  $\omega$  are Boltzmann constant, absolute temperature, resonance frequency and driving frequency of cantilever respectively. By this way, the stiffness of cantilever can be achieved by fitting the experimentally obtained thermal resonance curve and the theoretically calculated thermal Brownian noise. Figure 2.9 shows the calibration of typical tungsten cantilever by this method. The stiffness of this W cantilever is calculated as (53 N/m).

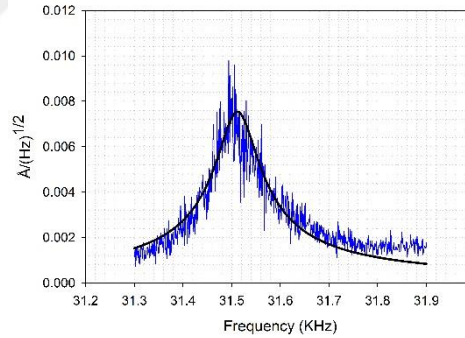


**Figure 2.9 :** Fit of the thermal resonance curve of the W cantilever on the Brownian noise curve, calculated stiffness of  $k \approx 53$  N/m.

### 2.3.3 Channels of microscope

In our small amplitude simultaneous AFM/STM system, beside the STM topography that is obtained using the tunnel current as feedback, by use of a Lock-in Amplifier, at the desired frequency (below resonance) oscillation amplitude and phase difference are measured and consequently force gradient and energy loss images are obtained.

Moreover, by recording the amplitude of the sinusoidal variation of the tunnel current using a second Lock-in Amplifier, the distance derivative of the tunnel current, which is a measure of the tunnel barrier height, can be obtained.

The use of very small oscillation amplitude, beyond enabling true simultaneous operation of AFM and STM, is necessary to make direct and quantitative force / force gradient measurements. For directly measuring of the short-range forces (such as covalent bonding) which is in order of a few Ångstrom, and known as the source of the atomic resolution imaging, use of the small amplitude oscillations (at least sub-Ångstrom) is unavoidable. By use of the sub-Ångstrom oscillation amplitude, the direct calculation of the force / force gradient from the measured signal of amplitude or frequency modulation is as easy as following equation:

$$k_{int} = -\frac{dF}{dz} = k_{lever} \left(1 - \left(\frac{\omega}{\omega_0}\right)^2\right) \left(\frac{A_0}{A} \cos\varphi - 1\right) \quad (2.9)$$

Where  $k_{lever}$  is the cantilever stiffness,  $\omega_0$  and  $\omega$  are resonance frequency and driving frequency of cantilever,  $\varphi$  is the phase shift,  $A_0$  is the free oscillation amplitude i.e., far from surface, and  $A$  is the measured amplitude where the tip is in interaction regime [45]. When the system is operating far from resonance frequency, the terms related to the driving frequency and phase shift are ignorable and the relationship can be written as;

$$k_{int} = -\frac{dF}{dz} = k_{lever} \left(\frac{A_0}{A} - 1\right) \quad (2.10)$$

The phase difference between the oscillations of the drive and the cantilever is a measure of the energy loss during an oscillation cycle. The tip-surface interaction energy loss to a good approximation is given by equation 2.11 [47] as;

$$E_{loss} = \frac{2\pi P_{int}}{\omega} = \frac{\pi}{4} k_0 A_0 A \sin\varphi \quad (2.11)$$

Where  $\omega$  is the lever oscillation frequency and  $\varphi$  is the phase difference between driving signal and the actual lever motion. This expression using the measured oscillation amplitude and phase shift, allows us to calculate directly the energy loss during each oscillation.

Two lock-in amplifiers accompany the system. One of them is used for measuring the oscillation amplitudes of the lever, which is mainly between 0.25—1.0 Å and the other one for recording tunnel current variations (dI) that is useful for measurement of tunnel barrier height and local density of states. If the response time of feedback loop is set



to high values than the oscillation period, the work function (tunnel barrier height) can be calculated by simultaneously recording of small oscillations in current during regular STM scanning. The work function (tunnel barrier height) can be calculated using equation 2.12;

$$\phi = 0.95(dI/I / dz)^2 \quad (2.12)$$

Both commercial Pt-Ir coated silicon cantilevers and homemade tungsten cantilevers are used, with spring constant range of almost 50 to 200 N/m. The spring constant is calculated from geometry and thermal oscillation measurements.

### **2.3.4 Force-distance spectroscopy**

To shed light on the contrast differences in imaging and to measure interactions such as force / force gradient between atoms, we have also accomplished what we call (F-d) spectroscopy measurements. On a certain point of sample by changing the distance between the surface and the tip, we can simultaneously measure the force / force gradient, as well as tunnel current, the tunnel barrier height as quantities in which we can determine their relationship with distance and each other.

## **2.4 Ultra High Vacuum Unit**

Our system is a commercial Omicron Ultra High Vacuum Scanning Probe Microscope that was modified and improved. The ultra-high-vacuum (UHV) chamber, shown in figure 2.10, is equipped with an argon-sputtering gun and a resistive heater used for sample/ lever preparation. The main chamber is pumped with a combination of an ion getter pump, titanium sublimation pump and a small turbo molecular pump backed with a double stage rotary pump. A base pressure range of  $2 \times 10^{-10}$  mbar is reached by baking out the chamber for at least two days at 120 degree of Celsius.



**Figure 2.10 : AFM/STM in Ultra High Vacuum.**

### 3. SYNTHESIS OF GRAPHENE

#### 3.1 CVD Grown Graphene

Graphene can be synthesized by Chemical Vapor Deposition (CVD). CVD has been proposed as most appropriate production method to achieve large area graphene [48]. As can be seen in figure 3.1, during thin film growth by Chemical Vapor Deposition (CVD) process, metal substrate (Copper) is heated up and precursor gases are released into the chamber and consequently a thin film is grown due to chemical reactions on the hot metal surface.

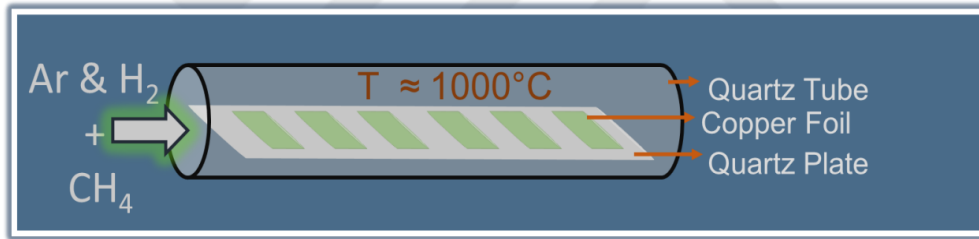


**Figure 3.1 :** Schematic of CVD process for growth of graphene on Cu foil.

Mostly, graphene lattice is produced by diffusing active carbon species such as CH or C. These active carbon species are formed by decomposing of methane or ethylene at the surface of hot metal. Two types of CVD growth have been introduced for graphene; atmospheric CVD and low pressure CVD. Different kinetics of growth lead to a variation in the uniformity of graphene. Moreover, it is worthwhile to be noticed that lowering methane concentration can result in production of monolayer graphene.

Graphene on various substrates are prepared by Dr. Oğuzhan Gürlü's group in their laboratory in Physics Department [49]. The graphene layers have been grown on the Cu foil by Chemical Vapor Deposition (CVD) method. Copper foils were heated up to a temperature of 1000°C under atmospheric pressure and annealed at this temperature under Hydrogen-Argon atmosphere to eliminate native-oxide layer and increase grain

sizes in copper. Following the annealing, methane was let into the tube with a very small flow rate compared to Argon & Hydrogen to grow graphene.

### 3.2 Transferring of CVD Grown Graphene on SiO<sub>2</sub>

Transferring of CVD grown graphene on non-conductive substrates could be helpful to minimize the effect of metallic substrate on the electronic behavior of graphene during the investigation by STM and AFM. The method was used to transfer of graphene on SiO<sub>2</sub> is displayed in figure 3.2. This technique is based on the use of polymethyl-methacrylate (PMMA) layer to keep the graphene layers unfolded during the etching of copper surface.

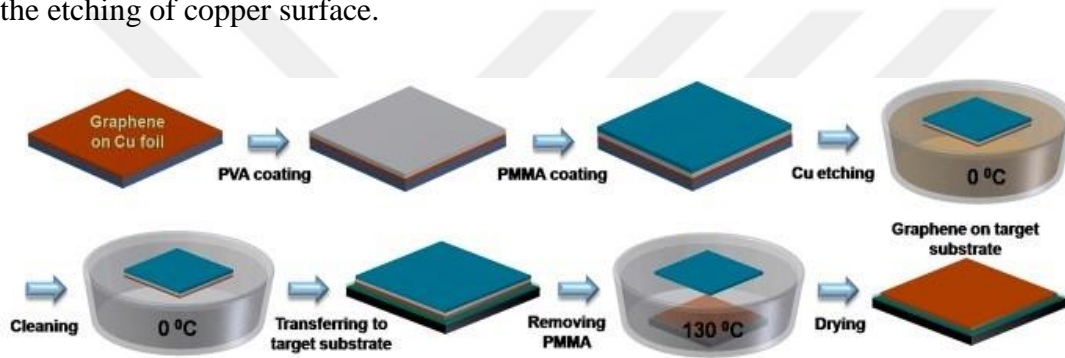


**Figure 3.2 :** Schematic shows PMMA technique, which is used to transfer graphene on the target substrate.

A layer of PMMA is coated onto the graphene. Then the metal catalyst is removed using an etchant. Therefore, the graphene stacked to the PMMA can be transferred to another substrate. Some solvents are then applied to separate the PMMA. However, it should be noted that transferring of graphene on non-conductive substrates without PMMA residues is unfeasible.

Figure 3.3 shows the Raman spectroscopy result of graphene after transferring onto SiO<sub>2</sub> wafer. The surface roughness and significant fluorescence background of copper substrate makes it difficult to analyse Raman spectrum of graphene. Accordingly, graphene after transferring onto SiO<sub>2</sub> wafer was taken to Raman spectroscopy measurement. Raman spectroscopy results support the growth of single layer and multilayer graphene on the Cu surface by region to region.

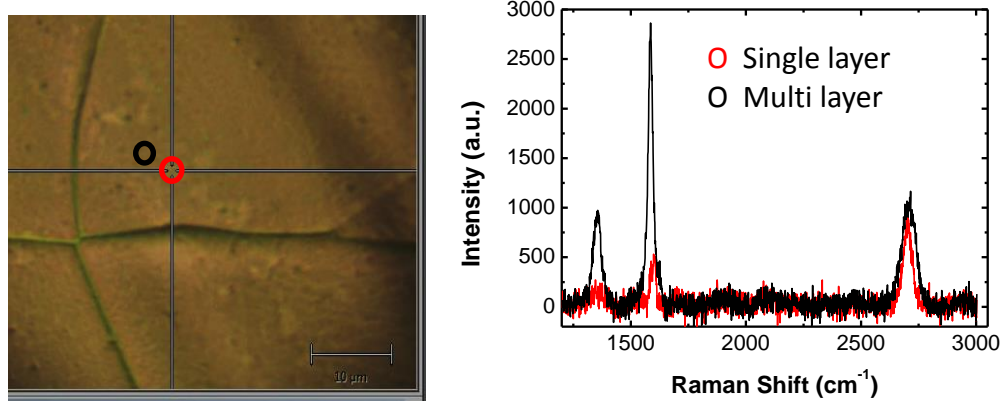


**Figure 3.3 :** Raman spectroscopy results of single layer and multilayer graphene transferred on SiO<sub>2</sub> wafer surface.



## **4. RESULTS AND DISCUSSION**

### **4.1 Graphene on Cu**

Investigation of graphene layers grown on the Cu foil has been accomplished by using simultaneous AFM / STM. Both commercial Pt-Ir coated Si cantilever and home-built Tungsten (W) cantilever were used. The constant tunnel current feedback is used in our small amplitude simultaneous AFM / STM system to obtain STM topography. Moreover, with the use of a Lock-in Amplifier set in the desired frequency (away from resonance frequency) and measurement of the oscillation amplitude and phase shift, the force gradient and energy dissipation images are obtained. In addition, the modulation in tunnel current is recorded using a second Lock-in Amplifier, which is used to extract the tunnel barrier height.

#### **4.1.1 Results obtained by Si cantilever**

Surface of copper is supposed to be covered by graphene during CVD growth. The large-scale scan of surface shows different steps that is considered as different steps on copper surface [figure 4.1.a]. STM topography image of lower layer demonstrates a honeycomb pattern that is assumed as a single layer graphene [figure 4.1.b,c]. Both honeycomb and trigonal patterns are seen in figure 4.1.d in two different regions. Two main interpretations can be evaluated for this particular image. The first one is a border of single layer and multilayer graphene. Inasmuch as we suppose that, the honeycomb pattern in single layer graphene and the trigonal pattern in multilayer graphene are appeared. In multilayer graphene, the maxima points in STM topography could be corresponded to A, B or hollow sites. The most reliable hypothesis is known as Bernal stacking that suggests carbon atoms of topmost layer are divided to two types of A and B atoms with different local density of states because of lattice mismatch with underneath graphene layer. In this hypothesis A atoms are located exactly above the carbon atom of underneath layer and B atoms are taken place above the hollow sites. They have different contribution to the local density of states in Fermi energy, where the tunnel current above B atoms are higher than A atoms. Consequently, during the

excitation of field states by applying bias voltage, the B atoms are supposed to be appeared as maxima points in STM topography images, which makes a trigonal pattern.

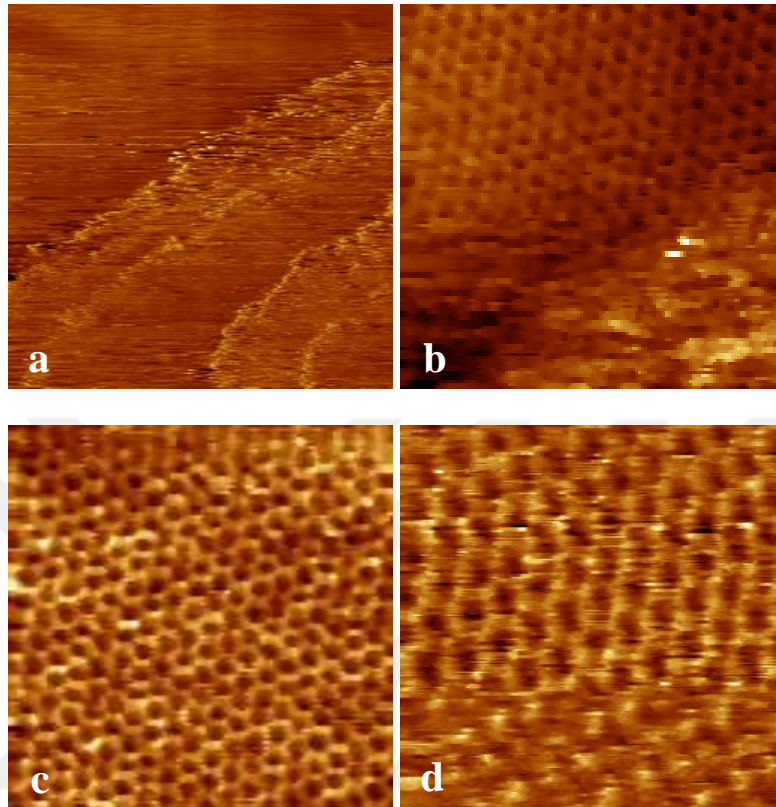


**Figure 4.1 :** STM topography images of (a) region with different steps, (b) and (c) upper region of image (a) which seems to be single layer graphene, (d) a region that both honeycomb and hexagonal pattern are observed that could be a border of single layer and multilayer graphene. Obtained using a Pt-Ir coated Si tip. Image sizes are  $380 \times 380 \text{ \AA}^2$ ,  $43 \times 43 \text{ \AA}^2$ ,  $43 \times 43 \text{ \AA}^2$  and  $29 \times 29 \text{ \AA}^2$  respectively.

Depending on the different experimental parameters, maxima points can be changed as A or hollow sites. Tip-surface distance and bias voltages are among the main reasons for these situations. Particularly, in the near to contact regimes, hollow sites are imaged as maxima points due to the saturation in tunnel current on carbon atoms. This case was observed in our obtained results where the trigonal pattern was appeared in STM topography at which its inversion converts to the honeycomb pattern [figure 4.2]. This means the hollow sites were imaged as maxima points.



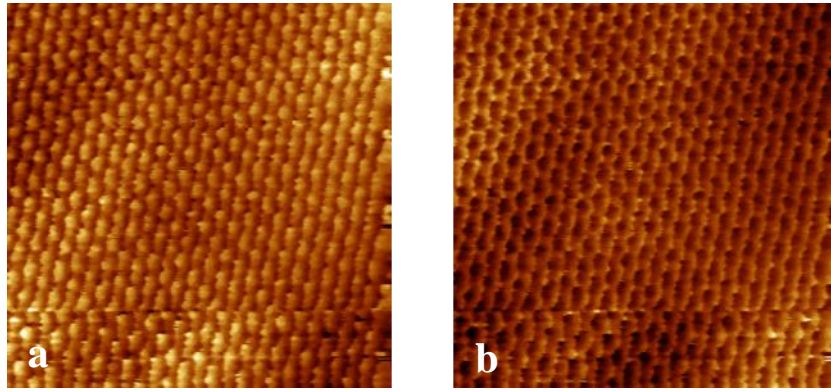


**Figure 4.2 :** (a) Trigonal pattern in STM topography (b) Honeycomb pattern in inverted contrast of STM topography. Obtained using a Pt-Ir coated Si tip. Image size is  $58 \times 58 \text{ \AA}^2$ .  $V_{\text{sample}} = -0.05 \text{ V}$ ,  $I_t = 0.2 \text{ nA}$ .

Tip changes during the scan can cause a contrast change in the topography image. Change of the effective atom in tunneling current or its breaking off from the tip are most probable events for the tip during the scan, which may result contrast differences. Effect of tip changes can be clearly seen in figure 4.3, where in topography image in two different line the contrast was changed abruptly. In two different regions of this image, we can see both trigonal and honeycomb structure. In the tunnel current modulation image, tip changes did not affect the overall contrast and we see the trigonal pattern in entire the area.

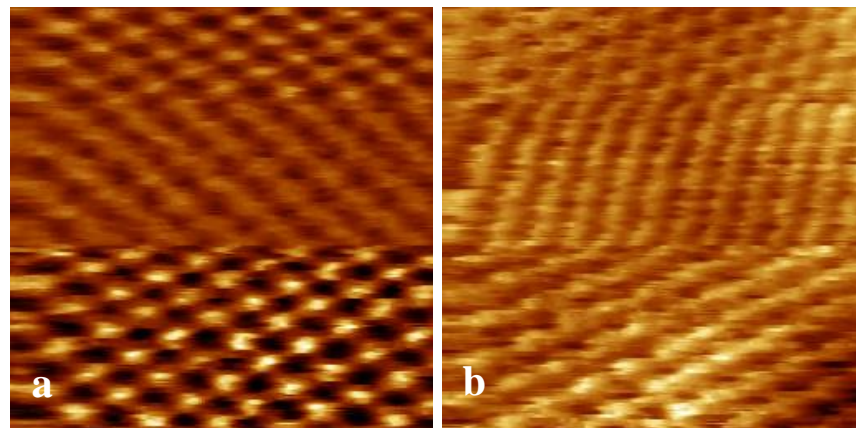


**Figure 4.3 :** Effect of tip changes during a particular scan is shown in (a) Tunnel current modulation and (b) STM topography images. Obtained using a Pt-Ir coated Si tip. Image size is  $29 \times 29 \text{ \AA}^2$ .  $V_{\text{sample}} = -0.15 \text{ V}$ ,  $I_t = 0.2 \text{ nA}$ , free amplitude  $A_0 = 0.41 \text{ \AA}_{\text{rms}}$ .

Honeycomb pattern in oscillation amplitude channel (inverted contrast of force gradient) and the same pattern in the inverted STM topography image were achieved as displayed in figure 4.4. We used commercial Pt-Ir coated Si cantilever with

approximated stiffness of 40 N/m. Imaging of hollow sites in STM topography (honeycomb in inverted contrast) suggests that tip-surface distance is very small. Moreover, as it will be discussed further, the force-distance spectroscopy measurements suggests that the scan of graphene on Cu was carried out in fully repulsive regime since we use tunnel current as our feedback parameter and tunneling regime is restricted in that regime.

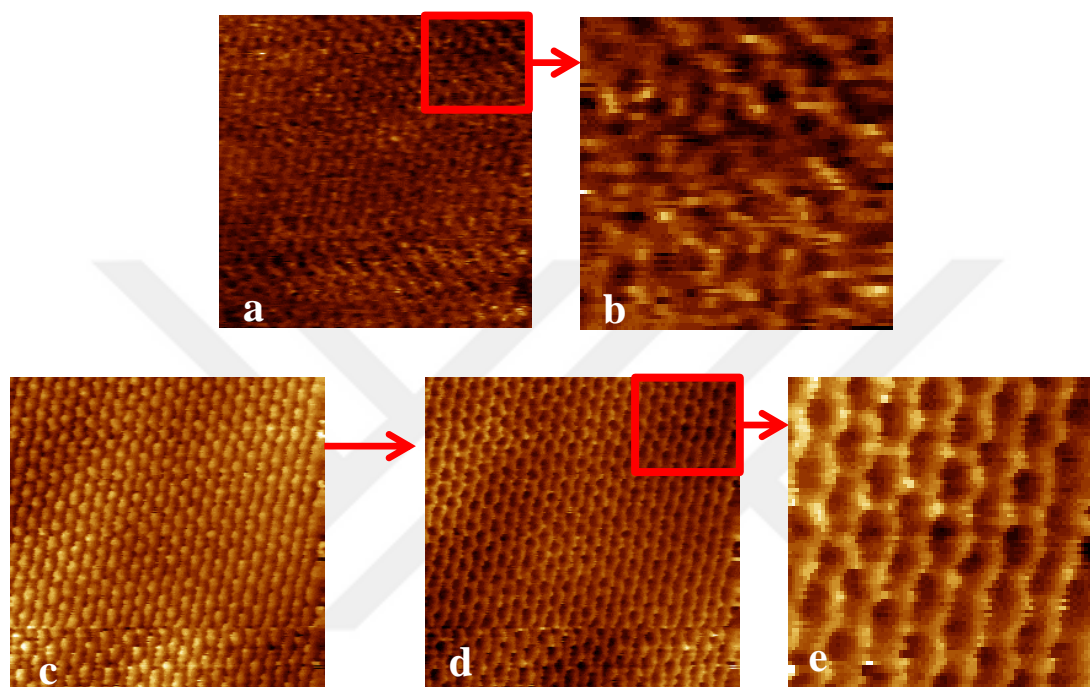


**Figure 4.4 :** Simultaneous AFM/STM images of graphene surface. (a) Oscillation amplitude (inverted contrast of force gradient) in constant tunnel current mode (b) Zoomed region of oscillation amplitude image (c) STM topography in constant current mode (d) Inverted contrast of STM topography (e) Zoomed region of inverted STM topography image. Obtained using Pt-Ir coated Si cantilever.  $f = 51.4$  kHz. Image size is  $58 \times 58 \text{ \AA}^2$ .  $V_{\text{sample}} = -50 \text{ mV}$ ,  $I_t = 0.2 \text{ nA}$ , free oscillation amplitude  $A_0 = 0.354 \text{ \AA}_{\text{rms}}$ .

Taking into account that the scan of surface was accomplished in fully repulsive regime, honeycomb pattern in oscillation amplitude channel shows that carbon atoms are less repulsive than hollow sites. It is not in good agreement with Pauli exclusion law. However, tip reactivity plays an important role in the contrast of force channels. Ondráček and his colleagues considered the different tip types and their effect on the contrast of force image [25]. They show that different tip types (Si and metallic tips) may have different force behavior on the carbon atoms and hollow sites that can change the contrast of force image. In our case, Pt-Ir coated Si cantilever seems to have less repulsive interaction on the carbon atoms compared to the hollow sites.

Based on the theoretical calculation, this behavior can only be observed for the case of Si tip. Our obtained result combined with the theoretical calculation suggest that the topmost atoms of our tip should be Si instead of Pt or Ir.

Figure 4.5 shows simultaneously obtained high-resolution AFM/STM images of the graphene surface. These images have been obtained using Pt-Ir coated Si cantilever. Atomic resolution has been obtained for all channels. In the inverted contrast of STM topography, three of the six atoms in the graphene hexagonal structure appear higher than the other three. As mentioned earlier, B atoms are often seen as bright points in the STM images due to the dominance of their electronic structure. However, it is important to note again that there are theoretical studies indicating that hollow sites can be observed as maxima points at very close tip-surface distances [25]. Determination of such differences in contrast, is quite difficult for very symmetrical and perfect surfaces such as graphite and graphene. Ondráček et al. in their reported theoretical study, considered the tunnel current behavior on three different sites depending tip-surface distance. They showed, in relatively long distance ( $\sim 5 \text{ \AA}$ ) from surface, B atoms have the maximum value for tunnel current. While, in relatively small distances, the A and hollow atoms can provide higher values for tunnel current. In particular, when the distance is approximately  $4 \text{ \AA}$ , the tunnel current above hollow atoms has greater value than A and B atoms. In addition, in very close region ( $\sim 3 \text{ \AA}$ ), the tunnel current on A and hollow sites have greater value than B atoms. The main reason provided for this behavior is the saturation in tunnel current above carbon atoms in very small distances to the surface. In the presented STM topography, two sites (most probably A and hollow sites) were imaged as bright points. The various f-d measurements indicate that during the scan of surface using typical Si cantilever and in almost all the variable set parameters, the operating region is restricted in fully repulsive force regime. This means the distance between tip and surface during the scan is very small and saturation in tunnel current in most of the experiments is inevitable. The inverted contrast of STM topography is shown in figure 4.6, where the maxima points are interpreted as B atoms.

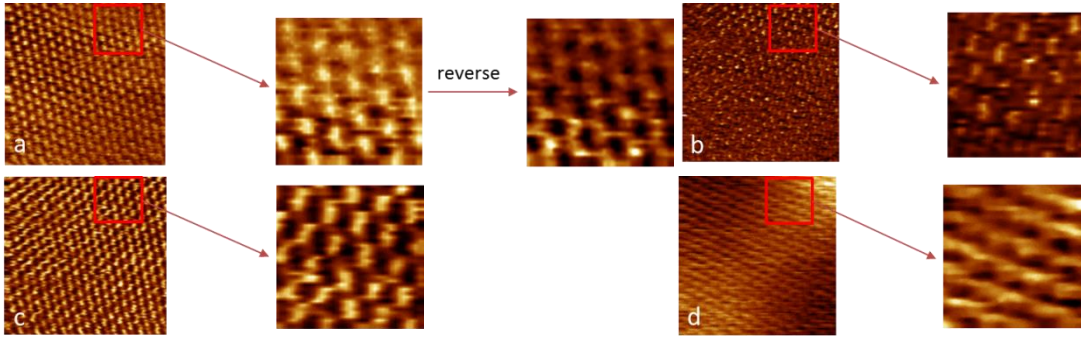


**Figure 4.5 :** Simultaneous AFM / STM images of Graphene surface and the corresponded zoomed regions. (a) Tunnel current modulation amplitude (measure of the tunnel barrier height), the inverted contrast was displayed as well. (b) Oscillation amplitude (inverted contrast of force gradient) (c) Phase shift (measure of energy loss) (d) STM topography, Obtained using Pt-Ir coated Si cantilever.  $k = 40 \text{ N / m}$ ,  $f = 47 \text{ kHz}$ , Image size is  $44 \times 44 \text{ \AA}^2$ .  $V_{\text{sample}} = 0.2 \text{ V}$ ,  $I_t = 0.17 \text{ nA}$ , free oscillation amplitude  $A_0 = 0.56 \text{ \AA}_{\text{rms}}$ .

In such a simultaneous scanning, there is a few pixels difference between the channels directly recorded by electronic unit and the channels recorded using lock-in amplifier. This depends on the selected bandwidth of lock-in amplifier and scan speed, which also can be calculated. In particular, in the images that are displayed in figure 4.5, the delay in the tunnel current modulation amplitude and the oscillation amplitude images is about two pixels. In addition, thermal shift induced distortion can often be seen in the scanning probe microscopy, especially in relatively slow scans. The selected regions in figure 4.5 were enlarged and are presented in figure 4.6. The horizontal position of the atoms in enlarged images were filtered through methods such as median filtering to be well defined. Moreover, graphene lattice model was placed on each image for better understanding of the relative positions of the atoms. The above-mentioned pixel shift was taken into account when the process has been done. Assuming the bright atoms in inverted contrast of STM image (according to the discussed interpretation in previous paragraph) as beta (B) atoms then the brightest points in the oscillation amplitude are the alpha (A) atoms as well. Based on the various force-distance spectroscopy experiments, the scanning being acquired in high repulsive force regime. At this regime, a higher oscillation amplitude correspond to the lower interaction stiffness and repulsive force. Accordingly, the interaction force on the hollow sites is more repulsive than both A and B types of carbon atoms. The interaction stiffness for A, B and hollow sites was extracted from oscillation amplitude data using equation 2.10. The values for A, B and hollow atoms are calculated as 373 N/m, 265 N/m and 401 N/m respectively. Again, it is in good agreement with the result



of the theoretical study reported by Ondráček et al. [25] for the contrast of Si tip on the carbon surface in AFM. However, comparison of A and B atoms indicates that interaction force on B atoms is relatively less repulsive than A atoms. Moreover, the tunnel current barrier height on A, B and hollow atoms was calculated from tunnel current modulation data using equation 2.12. The extracted values are 2.32 eV, 1.1 eV and 1.95 eV for A, B and hollow atoms respectively. It should be noted that the related experiment has been accomplished in constant current mode and consequently, the effect of tip trajectory is inevitable in the calculated values for interaction stiffness and barrier height. The different mechanical and electronic characteristics of A, B atoms, and the tip trajectory during the scan in constant current mode, may play roles in such a difference. Assuming not too much difference in terms of interaction force between A and B atoms during scanning in constant height, the force behavior for both A and B atoms is expected to be same.

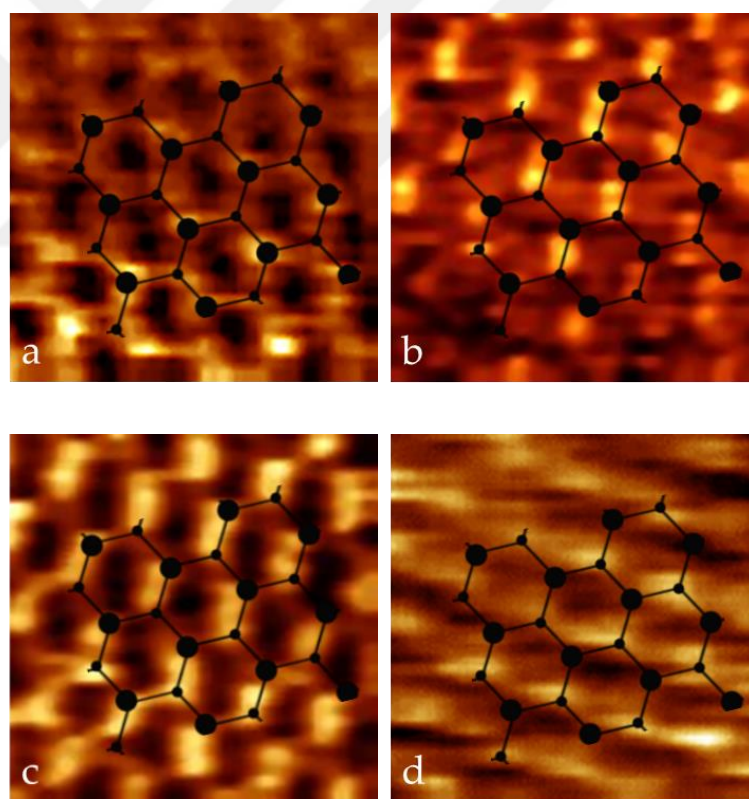


**Figure 4.6 :** Honeycomb models overlaid on the selected regions shown in Figure 4.5 (a) Inverted contrast of tunnel current modulation amplitude (b) Oscillation amplitude (inverted contrast of force gradient) (c) Phase shift (measure of energy dissipation) (d) Inverted contrast of STM topography.

The similar experiments have been done with opposite bias voltages to shed light on the contrast of STM and force gradient images. Simultaneous AFM / STM images in

opposite bias voltage obtained by Pt-Ir coated Si cantilever are displayed in figure 4.7. At this stage, we will particularly focus on the oscillation amplitude, which is a measure of force gradient and STM topography images. Solid circles in the atomic lattice model placed by the way to coincide with the bright atoms in the oscillation amplitude image, other images are also adopted to the relative position of this model. In the STM image, although tip-surface distance is very small and the probable changes in tip structure is the source of distortion, it seems to be possible to make comparisons. Again, the same behavior can be seen in STM topography and oscillation amplitude images. At this experiment, the triangular pattern can be seen in STM image. If we accept the bright points in STM topography as B atoms, the brightest points in the oscillation amplitude image corresponds to A atoms. This means the interaction force on B atoms is more repulsive than A atoms. It means the tip trajectory due to scan in constant current mode does change the force behavior on A and B atoms.

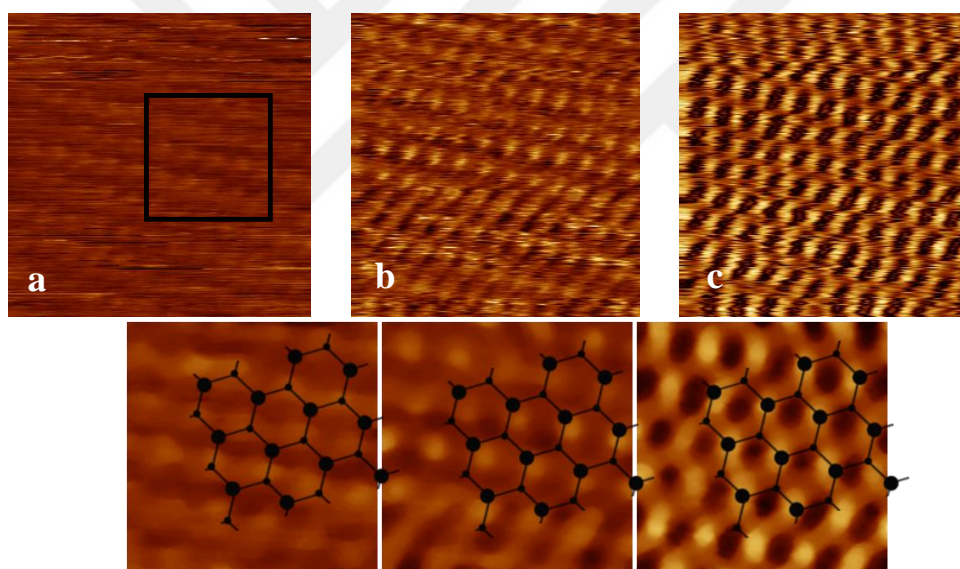


**Figure 4.7 :** Simultaneous AFM / STM images of the graphene surface. (a) STM topography (b) tunnel current modulation amplitude (measure of the tunnel barrier height) (c) oscillation amplitude (inverted contrast of force gradient). The following series are enlarged areas of frame shown in (a). Elements such as lateral shift and pixel delay has been corrected in the images. Obtained using Si cantilever.  $f = 51.4$  kHz. Image size is  $29 \times 29 \text{ \AA}^2$ .  $V_{\text{sample}} = -70 \text{ mV}$ ,  $I_t = 0.2 \text{ nA}$ , Free amplitude  $A_0 = 0.31 \text{ \AA}_{\text{rms}}$ .

The different mechanical characteristics of these carbon atoms is supposed to be another effective factor in their different force behavior. As previously mentioned, in graphene surfaces consisting of two or more layers, A atoms locating atop the carbon atoms and B atoms right in the hollow sites of the underlying graphene layer.

Therefore, atomic relaxation for these two types of carbon atom in the repulsive regime can be different and may result in such a difference in interaction force.

Our simultaneous STM/AFM microscope gives us the opportunity to consider atomic contrasts in more than one channel at the same time. Particularly, in the force-distance ( $f/d$ ) spectroscopy, on a particular point on the surface, by changing the distance between the tip and surface we can simultaneously measure force, force gradient, tunnel current and tunnel barrier height. This allows us to determine the relationship of these interactions with distance and with each other. It provides information on the magnitude of the effective force at a certain scanning condition, which plays an important role in AFM contrast mechanism. An example of this measurement is given in figure 4.8, which was obtained using the Pt-Ir coated Si cantilever on the graphene surface.

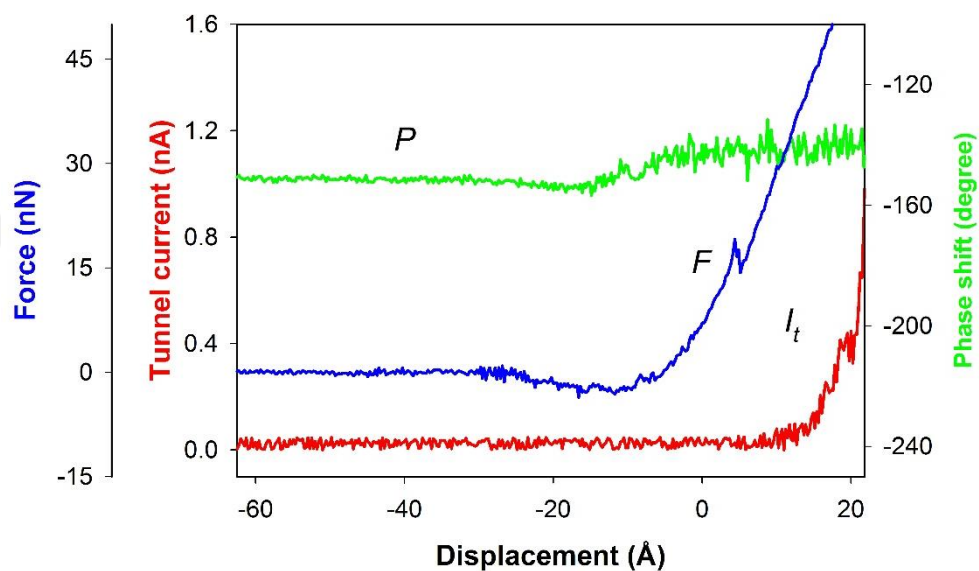


**Figure 4.8 :** F-d Spectroscopy. The Force, Phase shift and tunnel current curves as a result of sample displacement. Obtained by Si cantilever with the stiffness of (40 N/m) on the graphene surface.  $f= 47$  kHz.  $f_0= 156940$  Hz.  $A_0 = 0.48$  Å rms  $V_{\text{sample}} = -0.3$  V.

These curves show roughly the expected behavior when considering by their own. Tunnel current shows the exponential change depending the distance. The force as expected after reaching the maximum in attractive region goes to zero and thereafter continues to increase in the repulsive region. However, when we compare the range of interactions in the tunnel current, and force / force gradient, we see a different situation compared to many other examples. Based on some previous works that were carried

out on Si (111), Si (100) and Cu (100), the interaction for the tunnel current and force gradient start at about same distance. Therefore, the typical set tunnel current value in the STM has enabled us to study in the desired attractive or repulsive force regions. The situation in the measurements on graphene surface is very different. The interaction stiffness and force interaction begin far away from the tunnel current. In our simultaneous STM/AFM system, where we set a tunnel current to control the tip-surface distance, even a modest 0.1-0.2 nA current is as very high as to be taken in the repulsive force region. This makes imaging very difficult due to high force interaction between the tip and surface. More importantly, it shows, just how much tip and surface atoms are exposed to big forces during the STM operations and can even replace during imaging. Such interpretations of the role of force and theoretical calculations have been argued since the invention of STM, it is once again supported by our experiments on graphene surface.

Constant height mode scanning was also conducted, since it is thought to provide a perspective about the contrast mechanism of the force / force gradient images. In order to evaluate the consistency of the images obtained with constant height mode, while using the tunnel current as a feedback for the forward scan in each scan line, constant height mode (feedback off) is used on the backward scan. Therefore, force/force gradient images are obtained for the same region in two different scan modes (constant height / constant tunnel current). As shown in figure 4.9, the contrast of the oscillation amplitude image obtained in constant height mode does not show a significant difference in contrast compared to the one obtained in constant current mode.

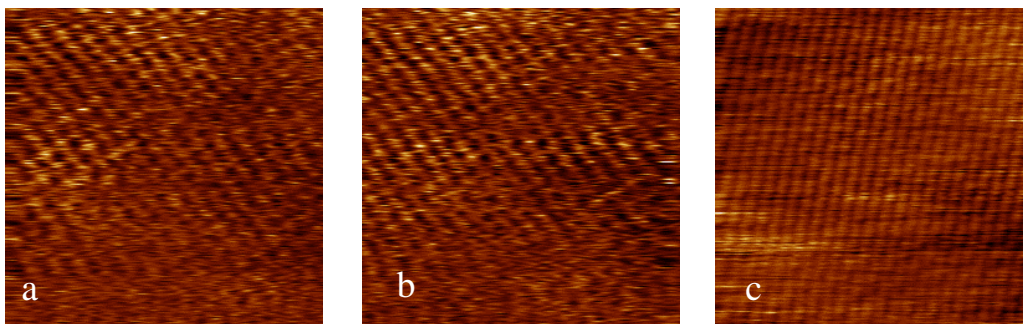


**Figure 4.9 :** Simultaneous AFM/STM images of graphene surface. (a) Oscillation amplitude in constant current mode (b) Oscillation amplitude in constant height mode (c) STM topography in constant tunnel current mode (d) STM topography in constant height mode. Obtained using Si cantilever.  $f = 51.4$  kHz. Image size is  $58 \times 58 \text{ \AA}^2$ ,  $V_{\text{sample}} = 50$  mV,  $I_t = 0.2$  nA, free oscillation amplitude  $A_0 = 0.32 \text{ \AA}$  rms.



### 4.1.2 Results obtained by W cantilever

We used homemade tungsten cantilever to scan the graphene surface using our simultaneous STM/AFM system. Previously we used Pt-Ir coated Si cantilever. It caused some uncertainty in interpretation of force interaction between graphene carbon atoms and dominant atom of tip as Pt, Ir or Si. Thus, using Tungsten cantilever, as a pure metallic tip, is helpful to study the both electronic and force behavior of carbon atoms in graphene surface. The large area scan of surface, as shown in figure 4.10, demonstrates the different steps on the surface of copper. These steps can be assumed as the steps on the polycrystalline copper surface. The surface of copper is mainly covered by the graphene. Since the graphene prohibit the copper surface from oxidization, these steps can be observed. Over the each step, graphene was formed as single layer and multilayer in different regions. The small area scan of surface over the each step provides the possibility to investigate the graphene in atomic scale.

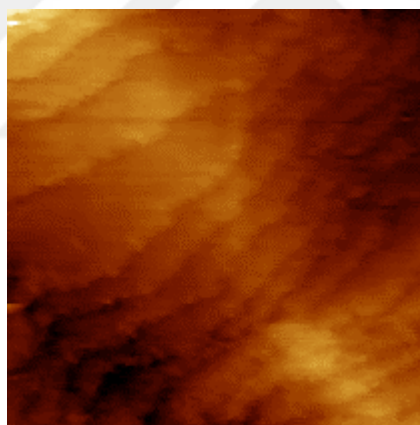


**Figure 4.10** : STM image of Graphene surface on Cu substrate. Obtained using a W tip, image size is  $820 \times 820 \text{ nm}^2$ ,  $V_{\text{sample}} = -0.7 \text{ V}$ ,  $I_t = 0.2 \text{ nA}$ .

Atomic resolution images have been obtained with different parameters of experiments and in different regions of surface with various layers of graphene. The honeycomb pattern was obtained in oscillation amplitude (measure of force gradient), tunnel current modulation (measure of barrier height) and phase shift (measure of energy dissipation) channels. While, the simultaneously measured STM topography shows trigonal or honeycomb pattern depend on the set parameters of experiment and region of scan. The stiffness of cantilever has been measured in good approximation as  $53 \text{ N/m}$ . The calculated interaction stiffness image demonstrates honeycomb pattern

that is not changed by set parameters of experiment or region of scan. However, the set parameters of experiment such as bias voltage and tip-surface distance as well as different regions of scan with different number of graphene layers play important roles in the contrast of STM topography image. As previously stated, applying bias voltage to the tip or sample can change the contrast of topography since it's changing the tunnel current from the empty states to the filled states or vice versa. In addition, tip-surface distance is another important factor where in very close regions due to the saturation in tunnel current the hollow atoms are imaged as maxima points. But the most important one as widely discussed in previous sections, is the two graphene layers mismatch known as Bernal stacking that suggests carbon atoms of topmost layer are divided to two types of A and B atoms with different local density of states. Consequently, during the excitation of filled states by applying bias voltage, the B atoms are supposed to be maxima points in STM topography images, which makes a trigonal pattern.

Considering the Raman results, the surface of copper is believed to be covered with graphene. Both single layer and multi-layer graphene were observed accordingly in different regions. Figure 4.11 shows the boundary of the graphene sheet (ribbon) above the sublayer graphene. As previously discussed in the introduction, the edge of a typical graphene layer can be formed in two types of structures known as Armchair and Zigzag. What makes these images unique is the armchair structure at the edge of the graphene sheet, which is clearly visible in the STM topography image.

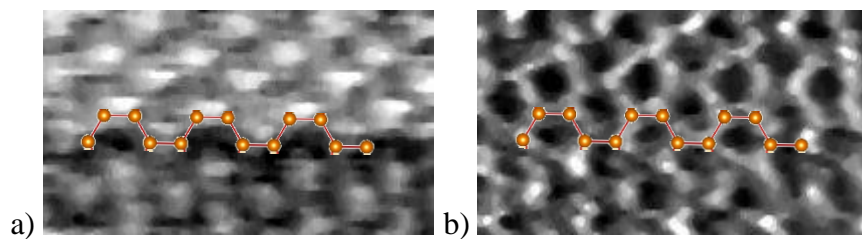


**Figure 4.11** : Simultaneous AFM/STM images of border of bilayer Graphene. (a) STM topography in constant current (forward scan) (b) Interaction Stiffness in constant height mode (backward scan). A pair of hexagonal unit cells is superimposed on the images. W cantilever of stiffness  $k = 53 \text{ N/m}$  and resonance frequency  $f_0 = 31.5 \text{ kHz}$ . Drive frequency  $f = 15 \text{ kHz}$ . Image size is  $18 \times 10 \text{ \AA}^2$ ,  $V_{\text{sample}} = 0.5 \text{ V}$ ,  $I_t = 0.6 \text{ nA}$ , Free amplitude  $A_0 = 0.3 \text{ \AA rms}$ .

The STM topography, tunnel current barrier height, energy dissipation and interaction stiffness images of graphene surface are displayed in figure 4.12. In this experiment,

all images were acquired simultaneously where during the scan we took off the feedback (constant current) for backward line to take the interaction stiffness images in both the constant current and the constant height modes.

The interaction stiffness images in both constant current and constant height modes show a honeycomb pattern demonstrating all six carbon atoms. Triangular pattern is seen in STM topography image. In this case, the inverted STM topography image converts to honeycomb pattern. This means that maxima points in the STM topography image belong to hollow sites. We supposed that tip-surface distance is in near to contact regime where the interaction between tip and carbon atoms is very high and probably due to the tunnel current saturation the STM topography shows the hollow sites as bright points rather than A or B atoms. It was estimated as a probability due to the tunnel current saturation on the carbon atoms in the very close regime [25]. In the interaction stiffness images, carbon atoms exhibit more positive values than hollow sites. This means that tip-surface distance during the imaging is close as much as to be beyond the force minimum.

Moreover, the force-distance spectroscopy measurements suggests that the scan of graphene on Cu is accomplished beyond the maximum attractive force since we use tunnel current as our feedback mechanism and tunneling regime is restricted in that regime. The values for interaction stiffness in both constant current (CC) and constant height (CH) scans were extracted from oscillation amplitude data using equation 2.9. The corrugation contrast between carbon and hollow sites is found to be 156 N/m and 148 N/m in, CC and CH modes respectively. Thus, the tip trajectory in CC mode has no significant effect on the measurement of interaction stiffness. In addition, the energy dissipation per oscillation cycle was calculated from phase shift data using equation 2.11. Energy dissipation on the carbon atoms are relatively higher than hollow sites. The average corrugation contrast between carbon atom and hollow site was measured as 0.1 eV in CH mode. Also, the tunnel current barrier height was extracted from tunnel current modulation data using equation 2.12. At this particular set tunnel current of 1.2 nA, the extracted barrier height values for carbon atom is relatively greater than one calculated for hollow sites. It is expected since at these set parameters and tip-surface distance (very close to the surface) due to the saturation in tunnel current on carbon atoms, the hollow sites were imaged as maxima points in

STM topography. The average corrugation contrast between carbon atom and hollow site is 1 eV.

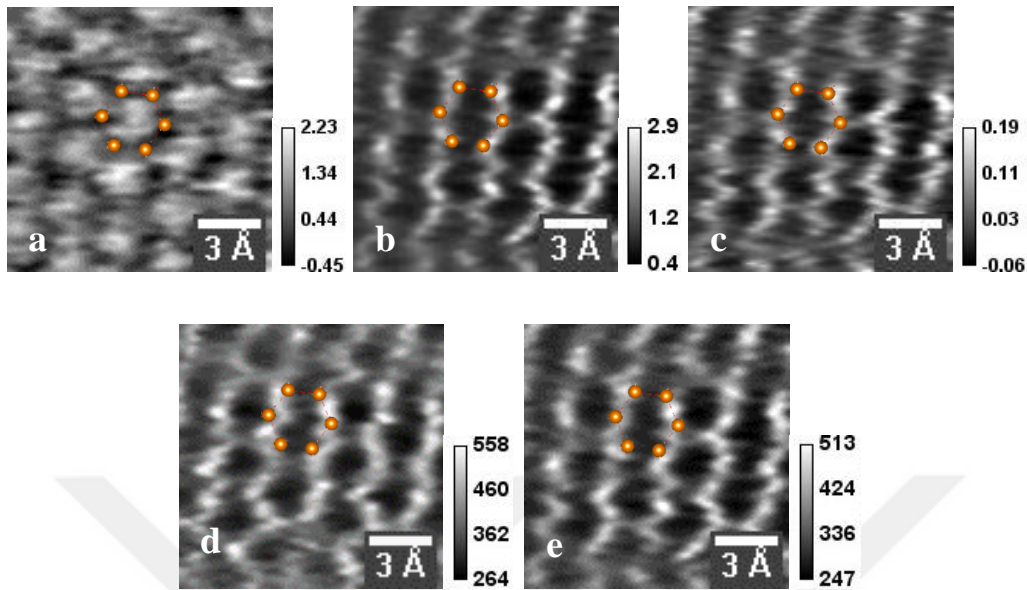


**Figure 4.12 :** Simultaneous AFM/STM images of Graphene surface on Cu substrate. (a) STM topography in constant current (forward scan) (b) Barrier height (eV) in constant height mode (backward scan). (c) Energy dissipation (eV) per oscillation cycle in constant height mode. (d) Interaction Stiffness in constant current mode (forward scan) and (e) Interaction Stiffness in constant height mode (backward scan). Scale bar values are in units of Å in STM and N/m in interaction stiffness images. Obtained with a W tip and cantilever of stiffness  $k = 53$  N/m and resonance frequency  $f_0 = 31.5$  kHz. Drive frequency  $f = 15$  kHz. Image size is  $11 \times 11$  Å<sup>2</sup>,  $V_{\text{sample}} = -0.5$  V,  $I_t = 1.2$  nA, Free amplitude  $A_0 = 0.3$  Å<sub>rms</sub>.

We scanned the same area with opposite bias voltage of 500mv while all the other parameters were taken same. The acquired results are shown in figure 4.13. As discussed previously, the contrast in STM topography can be inverted by applying opposite bias voltage since it is changing the tunnel current from the empty states to the filled states or vice versa. The inversion of STM topography contrast is clearly seen in the image showing the honeycomb pattern where carbon atoms are higher in contrast than the hollow sites. At this opposite bias voltage, the interaction stiffness images in both CC and CH shows the same behavior for carbon atoms and hollow sites where the honeycomb structure is seen in both of them. Although the contrast of interaction stiffness does not change at the opposite bias voltage, the values are relatively higher for carbon atoms and hollow sites, which means that the imaging was performed in a closer range to the surface.

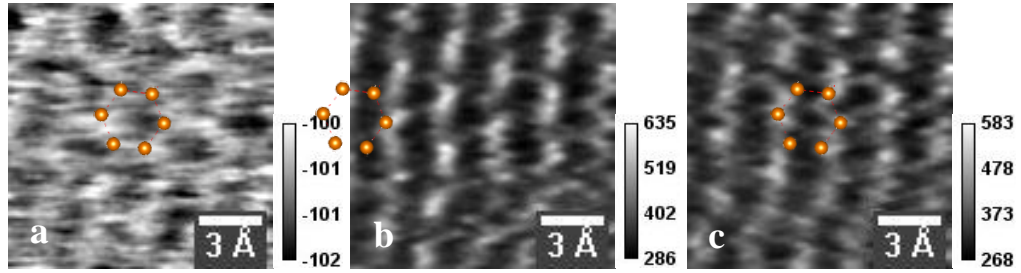


**Figure 4.13** : Simultaneous AFM/STM images of Graphene surface on Cu substrate. (a) STM topography in constant current (forward scan) (b) Interaction Stiffness in constant current mode (forward scan) and (c) Interaction Stiffness in constant height mode (backward scan). Scale bar values are in units of  $\text{\AA}$  in STM and N/m in interaction stiffness images. Obtained with a W tip and cantilever of stiffness  $k = 53$  N/m and resonance frequency  $f_0 = 31.5$  kHz. Drive frequency  $f = 15$  kHz. Image size is  $11 \times 11 \text{ \AA}^2$ ,  $V_{\text{sample}} = 0.5$  V,  $I_t = 1.2$  nA, Free amplitude  $A_0 = 0.3 \text{ \AA}_{\text{rms}}$ .

In some regions, STM topography demonstrates different contrast. Figure 4.14 shows an area with two specific regions. In STM topography image in the lower part, we see a trigonal pattern while at the top region the hexagonal pattern is seen. In this experiment, the set tunnel current is relatively lower and the interaction between tip and graphene is not so high means the tip-surface distance is not small enough to see the tunnel current saturation. Honeycomb pattern in force gradient shows that carbon atoms are repulsive than hollow sites. It is supposed as a single layer graphene that twisted or buckled. Therefore, due to the higher interaction between graphene and substrate (Copper) at the lower rather than upper region, the contrast of topography is changed by the dominance of substrate atoms. Moreover, the honeycomb structure in force gradient image and comparison with STM image demonstrates that the maxima points in simultaneously obtained STM image correspond to the middle of the carbon atoms (neither one nor the other). This cannot be concluded from a single STM image. The similar results were predicted by previous theoretical calculations for a sharp W tip in a specific range of bias voltages (0.3-0.7 V) [50].

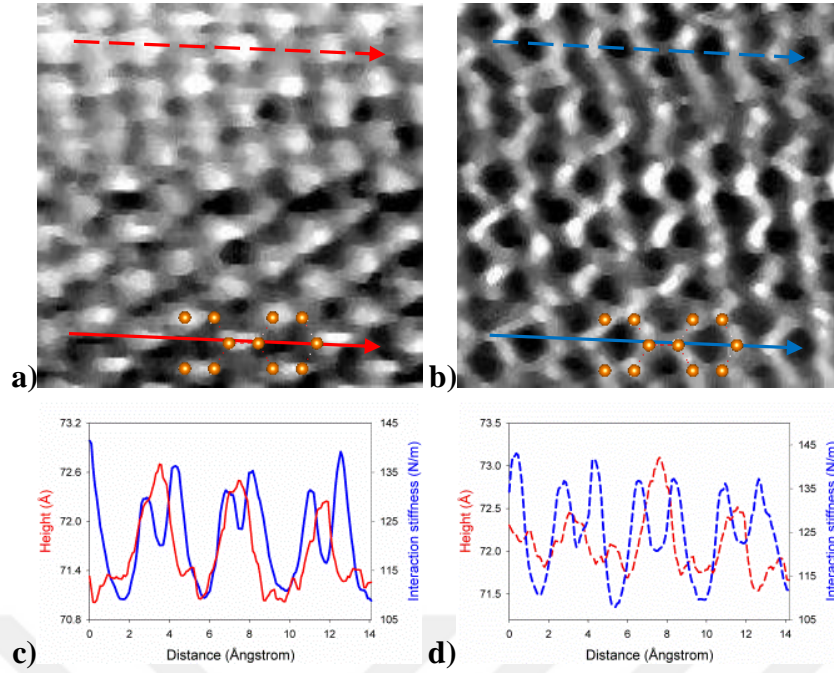


**Figure 4.14 :** Simultaneous AFM/STM images of Graphene surface. (a) STM topography in constant current (forward scan) (b) Interaction Stiffness in constant height mode (backward scan). A pair of hexagonal unit cells is superimposed on the images. The profiles along the indicated lines are given in (c) and (d). W cantilever of stiffness  $k = 53 \text{ N/m}$  and resonance frequency  $f_0=31.5 \text{ kHz}$ . Drive frequency  $f = 15 \text{ kHz}$ . Image size is  $18 \times 18 \text{ \AA}^2$ ,  $V_{\text{sample}} = 0.5 \text{ V}$ ,  $I_t = 0.6 \text{ nA}$ , Free amplitude  $A_0 = 0.3 \text{ \AA rms}$ .

The interaction regime is the most indicative factor on the imaging contrast of the different sites on the graphene surface. Using force-distance spectroscopy, the tunnel current and the force are simultaneously measured at a specific point on the sample, by changing the distance between the surface and the tip. Thermal drift makes it difficult to perform a site-specific spectroscopy at room temperature. We aimed to perform spectroscopy on a carbon atom and a hollow site. The thermal drift was minimized after a long time scan of surface. At this stage, several F-d curves were acquired by changing the lateral position of the tip over carbon and hollow sites. The force curves demonstrated two different behaviors that are believed to be taken at carbon and hollow sites. A group of F-d spectroscopy and the mean graph of two separate groups are shown in figure 4.15. Taking into account that the F-d measurements obtained at a specific set point for tunnel current, the curves obtained on the hollow site is replaced by  $2A$  derived from the STM topography image. The maximum attractive force for hollow site is about  $7 \text{ nN}$  while this value is about  $6 \text{ nN}$  for carbon atom. In previous theoretical calculations, the maximum attractive force



between a tungsten tip and both sites is reported about 2 nN [25]. However, the effect of electrostatic forces is not involved in such a study, which is inevitable in experimental measurements. In these measurements, the bias voltage of 500 mV was applied to the sample, which cause a huge electrostatic force. Furthermore, based on force-distance spectroscopy measurements, the images were mostly obtained while operating in repulsive interaction regime. We see the force interaction starts well before than the tunnel current. The constant tunnel current is used as feedback mechanism in our simultaneous STM/AFM. Obviously, even the modest tunnel current of 0.1-0.2 nA keeps the tip-sample interaction beyond the attractive regime.

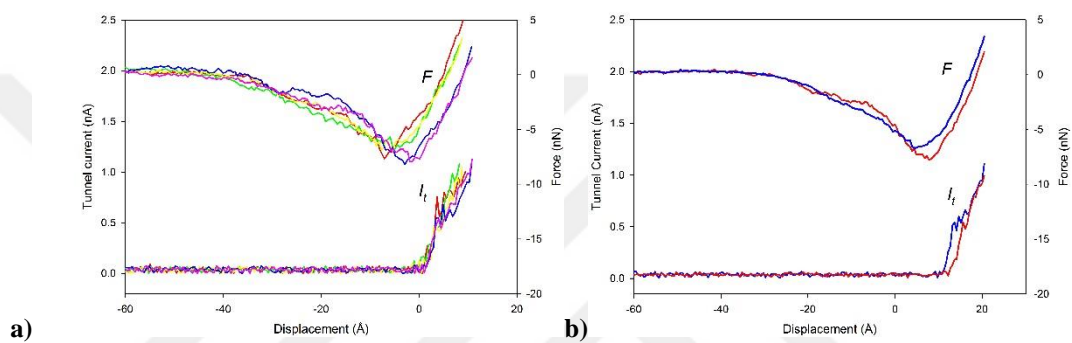


**Figure 4.15 :** F-d Spectroscopy. The Force ( $F$ ) and Tunnel current ( $I$ ) were measured as a function of relative tip-sample displacement, on a carbon site (blue curves) and hollow site (red curves). Obtained using the W cantilever used in imaging experiments, with stiffness of 53 N/m.  $V_{\text{sample}} = 0.5$  V.

The force-distance spectroscopy in negative bias voltage and comparison with the results obtained in positive voltages can shed light on the relative contrast of images acquired by STM and AFM. The similar F-d measurement to one discussed above was obtained in negative bias voltage as displayed in figure 4.16. In this case, the behavior of force interaction on the hollow site and carbon atom is similar to the one measured at positive bias voltage. The force interaction between tip and carbon atom starts earlier. However, for the tunnel current, it is clearly different where the tunnel current on hollow site and carbon atom start at the same distance. This was extracted from the images acquired at the similar bias voltages (-350 and -400 mV). Where at the set tunnel current of 0.4 nA, the contrast between carbon atoms and hollow sites can not be observed. It is important to note that the tunnel current for both carbon atom and hollow site could be a representative of saturation at the approximated value of (0.5-0.6 nA).

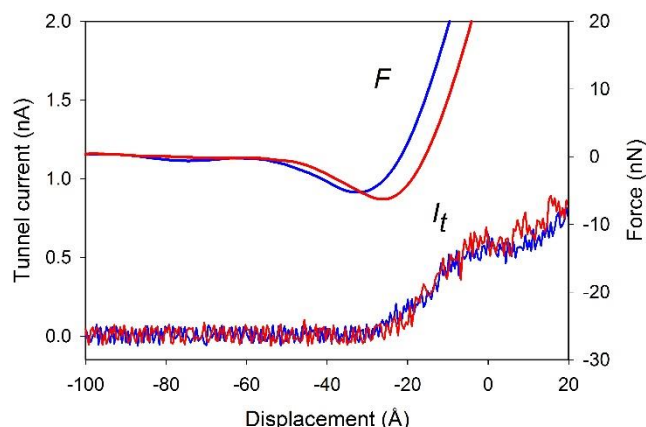


**Figure 4.16 :** F-d Spectroscopy. The Force ( $F$ ) and Tunnel current ( $I$ ) were measured as a function of relative tip-sample displacement, on a carbon site (blue curves) and hollow site (red curves). Obtained using the W cantilever used in imaging experiments, with stiffness of 53 N/m.  $V_{\text{sample}} = -0.35$  V.

The STM topography images at the similar bias voltages of (-350 and -400 mV) as well as a typical oscillation amplitude image at the related bias voltage are shown in figure 4.17. Honeycomb pattern was obtained in inverted contrast of oscillation amplitude (interaction stiffness) indicating the different behavior of interaction force on the carbon atoms and hollow sites. However, in the simultaneously obtained STM image, appreciable contrast difference between carbon atom and hollow site is not seen at the particular set tunnel current of 0.4 nA. This results support the above presented F-d curves. Where the tunnel current above carbon atoms and hollow sites shows similar behavior coinciding each other depending the distance to the surface.

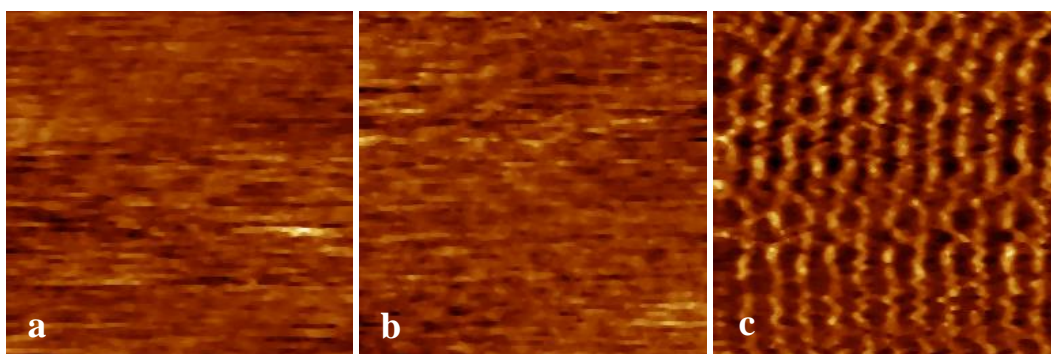


**Figure 4.17 :** AFM/STM images of Graphene surface. (a) STM topography in constant current mode with bias voltage of -0.35 V (b) STM topography in constant current mode with bias voltage of -0.4 V (c) Inverted contrast of oscillation amplitude (force gradient) constant current mode with bias voltage of -0.4 V. Obtained using W cantilever of stiffness  $k = 53$  N/m and resonance frequency  $f_0 = 31.5$  kHz. Drive frequency  $f = 15$  kHz. Image size is  $29 \times 29 \text{ \AA}^2$ ,  $I_t = 0.4$  nA, Free amplitude  $A_0 = 0.3 \text{ \AA}$  rms.



### **4.1.3 Comparison of results obtained by W and Si cantilevers**

The use of pure metal tips in non-contact AFM measurements is not common because the micro-fabricated cantilevers are limited to the Si cantilevers that are coated with metals such as Pt / Ir to obtain a metallic apex. However, there is doubt about the metallic nature of the tip if there is sufficient coating at the topmost apex of the tip and the survival of this coating during the experiments. Recently, Ondráček et al. [25] reported the results of the theoretical calculation on the contrast mechanisms of the carbon surfaces in AFM using different termination of Si tip and the metallic tips. In the case of the Si tip, the hollow sites shows more repulsive interaction than carbon atoms beyond the maximum attractive force, and that is opposite to the W tip, where the carbon atoms have more repulsive interaction than hollow sites beyond the the maximum attractive force. Our results obtained with Si and W tips are consistent with these calculations. However, In the Force-distance (F-d) measurement with W tip, the maximum attractive force for both sites are relatively higher (~ 6-7 nN) than the theoretical calculations where it is assumed to be about ~ 2 nN. During the experimental measurements, the effect of the electrostatic force is inevitable due to the applied bias voltage, which is the most important factor for such a difference in maximum attractive force, because in the theoretical calculations only the Wdv forces as long-range forces were taken into consideration.

## **4.2 Graphene Transferred on SiO<sub>2</sub>**

In addition to the works discussed above, simultaneous AFM / STM studies of CVD grown graphene that was transferred on SiO<sub>2</sub> using PMMA technique were accomplished. It is aimed to investigate the effect of Cu substrate on the graphene surface studies. Cu substrate is discussed to have two main effects on graphene surface studies. One of them is the Moire pattern-like structures resulting from the mismatching between the crystal structures of graphene and the Cu substrate. The other is an interaction that arises from the effect of high electron concentration of Cu on the local density of states (LDOS) of graphene, as remarkably observed in all

channels of AFM / STM. The results of simultaneous AFM / STM studies of graphene on SiO<sub>2</sub> are shown in figure 4.18.

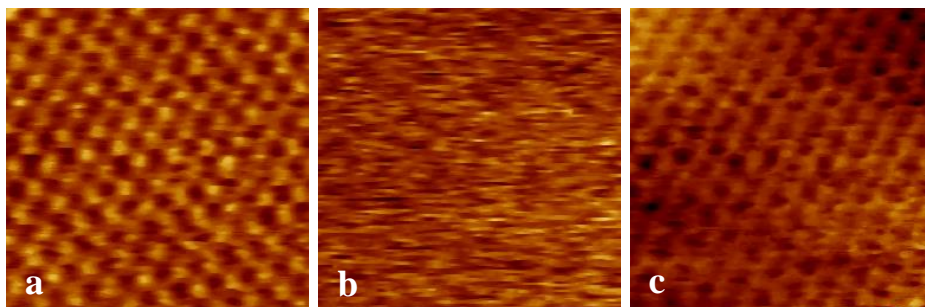


**Figure 4.18 :** Simultaneous AFM/STM images of graphene surface on SiO<sub>2</sub> (a) Tunnel current modulation amplitude (measure of the tunnel barrier height) (b) Oscillation amplitude (measure of force gradient) (c) STM topography obtained using Si cantilever.  $f = 18.340$  kHz. Image size is  $25 \times 25 \text{ \AA}^2$ .  $V_{\text{sample}} = -850$  mV,  $I_t = 0.15$  nA, free oscillation amplitude  $A_0 = 0.22 \text{ \AA}$  rms.

While STM topography and tunnel current modulation amplitude channels provide atomic resolution, oscillation amplitude (measure of force gradient) channel does not reveal any atomic structures. The main reason is the lower signal to noise ratio, which is not sufficient to obtain atomic contrast in force / force gradient channels. In the STM topography and tunnel current modulation (tunnel barrier height) channels, three of the six carbon atoms were imaged as bright points similar to the results obtained for graphene on Cu substrate. Hence, the most probable reason for imaging of the A and B atoms with different brightness (heights) in this experiment is the mismatch of the two graphene layers, one grown on top of the other.

### 4.3 Bismuth Telluride (Bi<sub>2</sub>Te<sub>3</sub>)

In addition, simultaneous AFM / STM studies on another two-dimensional material Bi<sub>2</sub>Te<sub>3</sub> surface are also performed. The Bi<sub>2</sub>Te<sub>3</sub> sample is prepared by cleaving a layer from Bi<sub>2</sub>Te<sub>3</sub> bulk sample.

High-resolution images of Bi<sub>2</sub>Te<sub>3</sub> surface were obtained by simultaneous AFM / STM, using Pt-Ir coated Si cantilever, which are shown in figure 4.19. The STM topography, tunnel current modulation and oscillation amplitude channels provide atomic resolution.

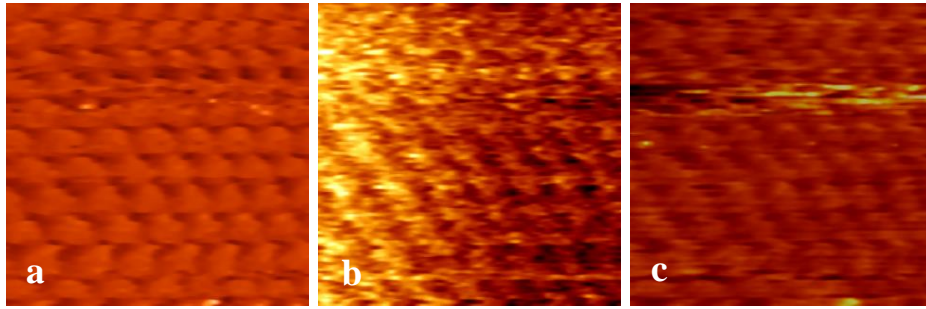


**Figure 4.19** : Simultaneous AFM/STM images of  $\text{Bi}_2\text{Te}_3$ . (a) Tunnel current modulation amplitude (measure of the tunnel barrier height) (b) Oscillation amplitude (measure of force gradient) (c) STM topography obtained using Si cantilever.  $f = 24.807$  kHz. Image size is  $35 \times 35 \text{ \AA}^2$ .  $V_{\text{sample}} = -1$  V,  $I_t = 0.25$  nA, free oscillation amplitude  $A_0 = 0.69 \text{ \AA}_{\text{rms}}$ .

$\text{Bi}_2\text{Te}_3$  is a two-dimensional material with trigonal lattice structure, where the lattice constant is  $4.38 \text{ \AA}$ , consistent with the obtained results.



## 5. CONCLUSIONS

We accomplished scan of graphene surface by our simultaneous AFM/STM for characterization of its structure at the atomic level. We used commercial Pt-Ir coated Si cantilever and home-made W cantilever. Analysis of results in different set parameters of experiment and different regions of surface with various layers of graphene has been done. Atomic resolution in almost all channels of microscope were obtained using both cantilevers. Honeycomb and trigonal patterns in STM topography in different regions were obtained. Besides, in the simultaneously acquired oscillation amplitude (measure of force gradient) and tunnel current modulation (measure of barrier height) and phase shift (energy dissipation) channels, honeycomb and trigonal patterns were obtained. Due to the shift and mismatch of successive layers, topmost layer of HOPG and multilayer graphene consists of three types of carbon atom known as A, B and hollow that provide different different local density of states. In previously reported STM studies on HOPG and multilayer graphene surface, in almost all the cases, the maxima points in trigonal structure of STM images were interpreted as B atoms, which have greater contribution to the density of states close to Fermi Energy. In our studies, F-d spectroscopy results obtained with Si cantilever show, in almost all of the experiments, the surface has been scanned during the operation in fully repulsive force regime. This demonstrates that tip and surface were in the very close proximity during the scan. In some cases, the hollow and A sites were imaged as bright points in STM topography instead of B atoms. This behavior has been predicted by Ondráček and his colleagues [25]. They showed in a theoretical calculation, when tip and surface are in very close distances, the opposite behavior can be observed in STM images and depend on the distance to the surface, hollow sites and in very small distances A and hollow sites can be imaged as maxima points in the STM topography. Our experimental results are a good example for this behavior. In addition, the carbon atoms are imaged in oscillation amplitude (inverted contrast of force gradient) channel. Considering the scan of surface in fully repulsive regime by using Pt-Ir coated Si cantilever, this is another unique behavior where repulsive interaction force on hollow sites is higher than carbon atoms. Ondráček et al. theoretically investigated the AFM

contrast of carbon surfaces with the use of different tip types (Si and metal tips) [25]. In the case of the Pt and Ir, the interaction force, beyond the force maximum, is more repulsive on carbon atoms compared to hollow sites, however, this behavior is more dominant for the case of Ir tip. In our case, Pt-Ir coated Si cantilever behaves more similar to the Si tips rather than Pt or Ir, where, beyond the force minimum, the interaction force on the hollow sites was more repulsive than carbon atoms. Accordingly, it can be concluded that the foremost atom in our cantilever is Si not Pt or Ir. In such metal coatings on Si cantilevers, there is already doubt on the quality of the coating and whether the coating survives during the operation of the microscope. The values for interaction stiffness on three different sites have been extracted from oscillation amplitude data. These values for sites A, B and hollow in a typical scan obtained in constant current mode using Si cantilever are found to be 373 N/m, 265 N/m and 401 N/m respectively. The difference in interaction stiffness between A and B atoms is interpreted as their different mechanical characteristics. Since A atoms are supposed to be located on top of the carbon atom of underneath graphene layer and B atoms are placed above the hollow site of the underneath layer, the different atomic relaxation, when they are exposed to such a huge repulsive interaction force, plays the most important role in the different interaction behavior of A and B types of carbon atoms.

Using tungsten cantilever, the honeycomb pattern is dominantly observed in force channels and both honeycomb and trigonal structures were seen in STM topography. Ondráček and his colleagues also reported the theoretical calculation of force behavior of W tip on the carbon atoms and hollow sites. Our experimental results are in perfect agreement with this theoretical study. In the case of tungsten cantilever, the hollow sites are imaged as bright points in oscillation amplitude (inverted contrast of force gradient) channel where the honeycomb structure can be obviously observed in the extracted interaction stiffness image, which is consistent with the theoretical calculation. The extracted interaction stiffness images obtained in constant current (CC) and constant height (CH) modes have the same contrast and the corrugation contrast between carbon atom and hollow site in CC and CH modes are found to be 156 N/m and 148 N/m respectively. The tip trajectory due to the constant current feedback does not significantly affect the measured interaction stiffness between tip and surface. Again, this indicates that using very small oscillation amplitudes can

provide the opportunity to have the true simultaneous STM/AFM. Moreover, in the extracted tunnel barrier height and energy dissipation images acquired in constant height mode, the corrugation contrast between carbon atom and hollow site was measured as 1eV and 0.1 eV, respectively. In the STM images, at the distances close to the surface, due to the tunnel current saturation, hollow sites were imaged as bright points, where the inverted contrast displays the honeycomb structure. Furthermore, the unique results have been obtained in the STM images. In the last decades, the STM images of HOPG and graphene showing a triangular pattern were interpreted as revealing either of the carbon atoms or hollow sites as brighter structures, depending on experimental parameters and tip structures. For the first time, we have experimentally shown that in the trigonal structure of the STM topography, the maximum points can correspond to the middle of the A and B atoms (neither one nor the other). Teobaldi et al. reported a theoretical study with the similar results for a sharp W tip for a specific range of bias voltages (0.3-0.7 V) [50]. This theoretical study clearly supports our experimental observations. It is important to mention that the simultaneously obtained AFM image provides the confidence of detecting this phenomenon in the STM image. Also, simultaneous operation as close as possible to true STM mode, is only possible with the use of sub-angstrom oscillation amplitudes.





## REFERENCES

- [1] Novoselov, K.S., Geim, A.K., Morozov, S.V., Jiang, D., Zhang, Y., Dubonos, S.V., Grigorieva, I.V., Firsov, A.A., (2004) Electric field effect in atomically thin carbon films, *Science* 306 666-9.
- [2] Novoselov, K.S., Geim, A.K., Morozov, S.V., Jiang, D., Katsnelson, M.I., Grigorieva, I.V., Dubonos, S.V., Firsov, A.A., (2005) Two-dimensional gas of massless Dirac fermions in graphene, *Nature* 438 197-200.
- [3] Geim, A.K., Novoselov, K.S., (2007) The rise of graphene, *Nat. Mater.* 6 183-91.
- [4] Binnig, G., Fuchs, H., Gerber, Ch., Rohrer, H., Stoll E. and Tosatti, E., (1986) Energy-dependent state-density corrugation of a graphite surface as seen by scanning tunneling microscopy, *Europhys. Lett.* 1 31.
- [5] Park, S., Quate, C.F., (1986) Tunneling microscopy of graphite in air, *Appl. Phys. Lett.* 48 112.
- [6] Cisternas, E., Stavale, F., Flores, M., Achete, C.A., Vargas, P., (2009) First-principles calculation and scanning tunneling microscopy study of highly oriented pyrolytic graphite (0001), *Phys. Rev. B* 79 205431.
- [7] Mizes, H.A., Park, S., Harrison, W.A., (1987) Multiple-tip interpretation of anomalous scanning-tunneling-microscopy images of layered materials, *Phys. Rev B Condens Matter* 36 4491-4494.
- [8] Ouseph, P.J., Poothackanal, T., Mathew, G., (1995) Honeycomb and other anomalous surface pictures of graphite, *Phys. Lett. A* 205 65.
- [9] Paredes, J.I., Martnez-Alonso, A., Tascon, J.M.D., (2001) Triangular versus honeycomb structure in atomic-resolution STM images of graphite, *Carbon* 39 476.
- [10] Wang, Y., Ye, Y., Wu, K., (2006) Simultaneous observation of the triangular and honeycomb structures on highly oriented pyrolytic graphite at room temperature: An STM study, *Surf. Sci.* 600 729.
- [11] Hölscher, H., Allers, W., Schwarz, UD., Schwarz, A. and Wiesendanger, R., (2000) Interpretation of “true atomic resolution” images of graphite (0001) in noncontact atomic force microscopy, *Phys. Rev. B* 62 6967.
- [12] Hembacher, S., Giessibl, F.J., Mannhart, J. and Quate, C.F., (2003) Revealing the hidden atom in graphite by low-temperature atomic force microscopy, *Proc. Natl. Acad. Sci. U.S.A.* 100 12539.
- [13] Ashino, M., Schwarz, A., Behnke, T., Wiesendanger, R., (2004) Atomic-resolution dynamic force microscopy and spectroscopy of a single-walled carbon nanotube: characterization of interatomic van der Waals forces, *Phys. Rev. Lett.* 93 136101.

- [14] **Albers, B.J., Schwendemann, T.C., Baykara, M.Z., Pilet, N., Liebmann, M., Altman, E.I., Schwarz, U.D.,** (2009) Three-dimensional imaging of short-range chemical forces with picometre resolution, *Nat. Nanotech.* 4 307-10.
- [15] **Chen, C.J.,** (1991) Attractive interatomic force as a tunneling phenomenon, *J. Phys. Condens. Matter* 3 1227.
- [16] **Schneir, J., Sonnenfeld, R., Hansma, P.K., Tersoff, J.,** (1986) Tunneling microscopy study of the graphite surface in air and water *Phys. Rev. B* 34 4979.
- [17] **Tomanek, D., Louie, S.G., Marnin, H.J., Abraham, D.W., Thomson, R.E., Ganz, E., Clarke, J.,** (1987) Theory and observation of highly asymmetric atomic structure in scanning-tunneling-microscopy images of graphite *Phys. Rev. B* 35 7790.
- [18] **Dedkov, Y., Voloshina, E.,** (2014) Multichannel scanning probe microscopy and spectroscopy of graphene moiré structures, *Phys. Chem. Chem. Phys.* 16 3894-908.
- [19] **Yıldız, D., Gürlü, O.,** (2016) Apparent corrugation variations on moiré patterns on highly oriented pyrolytic graphite, *Materials Today Communications* 8 72.
- [20] **Ouseph, P.J.,** (2000) Scanning tunneling microscopy observation of dislocations with superlattice structure in graphite, *Appl. Surf. Sci.* 165 38.
- [21] **Sun, H.L., Shen, Q.T., Jia, J.F., Zhang, Q.Z., Xue, Q.K.,** (2003) Scanning tunneling microscopy study of superlattice domain boundaries on graphite surface, *Surf. Sci.* 542 94.
- [22] **Coraux, J., N'Diaye, A.T., Busse, C. and Michely, T.,** (2008) Structural coherency of graphene on Ir (111) *Nano Lett.* 8 565.
- [23] **Pletikosić, I., Kralj, M., Pervan, P., Brako, R., Coraux, J., N'Diaye, A.T., Busse, C. and Michely, T.,** (2009) Dirac cones and minigaps for graphene on Ir (111) *Phys. Rev. Lett.* 102 056808.
- [24] **Allers, W., Schwarz, A., Schwarz, U.D. and Wiesendanger, R.,** (1999) Dynamic scanning force microscopy at low temperatures on a van der Waals surface: graphite (0001), *Appl. Surf. Sci.* 140 247.
- [25] **Ondráček, M., Pou, P., Rozsival, V., González, C., Jelínek, P., Pérez, R.,** (2011) Forces and currents in carbon nanostructures: are we imaging atoms?, *Phys. Rev. Lett.* 106 176101.
- [26] **Vaari, J., Lahtinen, J., Hautojärvi, P.,** (1997) The adsorption and decomposition of acetylene on clean and K-covered Co (0001) *Catal. Lett.* 44 43-49.
- [27] **Gamo, Y., Nagashima, A., Wakabayashi, M., Terai, M., Oshima, C.,** (1997) Atomic structure of monolayer graphite formed on Ni (111) *Surf. Sci.* 374 61-64.
- [28] **Land, T.A., Michely, T., Behm, R.J., Hemminger, J.C., Comsa, G.,** (1992) STM investigation of single layer graphite structures produced on Pt (111) by hydrocarbon decomposition *Surf. Sci.* 264 261-270.

- [29] **Ueta, H., Saida, M., Nakai, C., Yamada, Y., Sasaki, M., Yamamoto, S.,** (2004) Highly oriented monolayer graphite formation on Pt (1 1 1) by a supersonic methane beam *Surf. Sci.* 560 183-190.
- [30] **Starr, D. E., Pazhetnov, E. M., Stadnichenko, A. I., Boronin, A. I., Shaikhutdinov, S. K.,** (2006) Carbon films grown on Pt(1 1 1) as supports for model gold catalysts *Surf. Sci.* 600 2688-2695.
- [31] **Oshima, J., Nagashima, A.,** (1997) Ultra-thin epitaxial films of graphite and hexagonal boron nitride on solid surfaces *J. Phys.: Condens. Matter* 9 1.
- [32] **Marchini, S., Günther, S. and Winterlin, J.,** (2007) Scanning tunneling microscopy of graphene on Ru(0001) *J. Phys. Re.B* 76 075429.
- [33] **Gall', N. R., Rut'kov, E. V., Tontegode, A. Y.,** (2004) Interaction of silver atoms with iridium and with a two-dimensional graphite film on iridium: Adsorption, desorption, and dissolution *Phys. Solid State* 46 371-377.
- [34] **N'Diaye, A. T., Bleikamp, S., Feibelman, P., Michely, T.,** (2006) Two-dimensional Ir cluster lattice on a graphene moiré on Ir (111) *Phys. Re.Lett.* 97 215501.
- [35] **Makarenko, I. V., Titkov, A. N., Waqar, Z., Dumas, P., Rutkov, E.V., Gall, N. R.,** (2007) Structural properties of a monolayer graphite film on the (111) Ir surface *Phys. Solid State* 49 371-376.
- [36] **Dedkov, Y., Voloshina, E., Fonin, M.,** (2015) Scanning probe microscopy and spectroscopy of graphene on metals, *Phys. Status Solidi B* 252 451-468.
- [37] **Novoselov, K. S., Jiang, Z., Zhang, Y., Morozov, S. V., Stormer, H. L., Zeitler, U., Maan, J. C., Boebinger, G. S., Kim, P., Geim, A. K.,** (2007) Room-Temperature Quantum Hall Effect in Graphene *Science* 315 1379.
- [38] **Fujita, M., Wakabayashi, K., Nakada, K., Kusakabe, K.,** (1996) Peculiar Localized State at Zigzag Graphite Edge *J. Phys. Soc., Jpn.* 65 1920-1923.
- [39] **Nakada, K., Fujita, M., Dresselhaus, G., Dresselhaus, M.S.,** (1996) Edge state in graphene ribbons: Nanometer size effect and edge shape dependence *Phys. Rev.B* 54 17954-17961.
- [40] **Fernandez-Rossier, J., Palacios, J. J.,** (2007) Magnetism in graphene nanoislands *Phys. Rev. Lett.* 99 177204.
- [41] **Wang, W. L., Meng, S., Kaxiras, E.,** (2008) Graphene nanoflakes with large spin *Nano Lett.* 8 241-245.
- [42] **Oral, A., Grimble, R.A., Özer, H. Ö., and Pethica, J.B.,** (2003) High-sensitivity noncontact atomic force microscope/scanning tunneling microscope (nc AFM/STM) operating at subangstrom oscillation amplitudes for atomic resolution imaging and force spectroscopy, *Rev.of Sci. Inst.* 74 8.
- [43] **Herz, M., Schiller, Ch., Giessibl, F.J., and Mannhart, J.,** (2005) Simultaneous current-, force-, and work-function measurement with atomic resolution, *Appl. Phys. Lett.* 86 153101.

- [44] **Oral, A., Grimble, R.A., Özer, H. Ö., Hoffmann, P.M. and Pethica, J.B.,** (2001) Quantitative atom-resolved force gradient imaging using noncontact atomic force microscopy, *Appl. Phys. Lett.* 79 1915.
- [45] **Özer, H. Ö., O'Brien, S.J., and Pethica, J.B.,** (2007) Local force gradients on Si (111) during simultaneous scanning tunneling/atomic force microscopy, *Appl. Phys. Lett.* 90 133110.
- [46] **Fukuma, T., Kimura, M., Kobayashi, K., Matsushige, K., and Yamada, H.,** (2005) Development of low noise cantilever deflection sensor for multienvironment frequencymodulation atomic force microscopy *Rev. of Scien. Inst.* 76 053704.
- [47] **Hoffmann, P. M., Jeffery, S., Pethica, J. B., Özer, H. Ö., Oral, A.,** (2001) Energy Dissipation in Atomic Force Microscopy and Atomic Loss Processes *Phys. Rev. Lett.* 87 265502.
- [48] **Li, X., et al.,** (2009) Large-area synthesis of high-quality and uniform graphene films on copper foils, *Science* 324 1312.
- [49] **Kamber, U., Kincal, C., Yagci, B., Birer, O. and Gürlü, O.,** (2018) Silicon-based Fractal Structure Formation in Chemical Vapor Deposition Growth of Graphene on Copper Foils, (submitted for publication).
- [50] **Teobaldi, G., Inami, E., Kanasaki, J., Tanimura, K., Shluger, A. L.,** (2012) Role of applied bias and tip electronic structure in the scanning tunneling microscopy imaging of highly oriented pyrolytic graphite *Phys. Rev. B* 85 085433.

## CURRICULUM VITAE

**Name Surname** : Majid Fazeli Jadidi  
**Place and Date of Birth** : Tabriz / 31.03.1981  
**E-Mail** : fazelijadidi@itu.edu.tr

### EDUCATION

- **B.Sc.** : 2005, University of Urmia, Physics.
- **M.Sc.** : 2009, University of Zanjan, Physics.

### PUBLICATIONS, PRESENTATIONS AND PATENTS ON THE THESIS:

- **Jadidi, M. F.,** Kamber, U., Gürlü, O. and Özer, H. Ö., 2017: Investigation of Graphene using Simultaneous Scanning Tunneling/Atomic Force Microscopy 81st Annual Meeting of the DPG, March 2017 , Dresden, Germany.
- **Jadidi, M. F.,** Kamber, U., Gürlü, O. and Özer, H. Ö 2017: Characterization of Graphene using Simultaneous Scanning Tunneling/Atomic Force Microscopy, 13rd Nanoscience and Nanotechnology Conference, October 2017, Antalya, Turkey.
- **Jadidi, M. F.,** Kamber, U., Gürlü, O. and Özer, H. Ö., 2018 Investigation of CVD graphene as-grown on Cu foil using simultaneous Scanning Tunneling /Atomic Force Microscopy *Beilstein J Nanotechnol.* 9 2953-2959.

### OTHER PUBLICATIONS, PRESENTATIONS AND PATENTS:

- Kılıç, A., **Jadidi, M. F.,** Özer, H. Ö., Kök, F. N., 2017 The effect of thiolated phospholipids on formation of supported lipid bilayers on gold substrates investigated by surface-sensitive methods *Colloids and Surfaces B: Biointerfaces* 160 117-125.
- Sönmez, T., **Jadidi, M. F.,** Kazmanli, K., Birer, Ö., Ürgen, M., 2016 Role of different plasma gases on the surface chemistry and wettability of RF plasma treated stainless steel *Vacuum* 129 63-73.